

TM no. 51-78-18



TECHNICAL MEMORANDUM

title:

AN EVALUATION OF THE ACCURACY OF MATERIAL MODEL
REPRESENTATION OF REINFORCED CONCRETE *by J*

author:

J. M. Ferritto,

date:

July 1978, ¹¹

sponsor:

NAVAL FACILITIES ENGINEERING COMMAND

program

nos:

ZR000-01-164



CIVIL ENGINEERING LABORATORY

NAVAL CONSTRUCTION BATTALION CENTER
Port Hueneme, California 93043

Approved for public release; distribution unlimited.

NCEL
TM-
51-78-18

C.2.

CONTENTS

	Page
BACKGROUND	1
YIELD-STRESS MOMENT AND MOMENT OF INERTIA	3
ULTIMATE STRENGTH MOMENT CAPACITY	6
MODULUS OF ELASTICITY	8
ACI CODE APPROACH FOR COMPUTING MOMENT OF INERTIA FOR DEFLECTION	9
EQUIVALENT MODULUS APPROACH FOR COMPUTING DEFLECTION	10
NAVFAC P-397 APPROACH FOR COMPUTING MOMENT OF INERTIA FOR DEFLECTION	12
MODEL REINFORCED CONCRETE BEAMS	12
Tension Failures	13
Compression Failures	13
Shear Failures	13
ANALYSIS BY EQUIVALENT BEAM	14
Tension Failure	14
Compression Failure	15
Shear Failure	15
MATERIAL MODELS FOR COMPOSITE REPRESENTATION OF REINFORCED CONCRETE	16
Variable Modulus Model	17
Tresca Yield Condition Maximum Shear Theory	17
Von Mises' Yield Condition (Distortion Energy Theory)	18
Drucker-Prager Model	22
Mohr-Coulomb	26
ADINA Concrete Model	26
CONCRETE BEHAVIOR	27
MATERIAL MODELS AVAILABLE IN ADINA TO REPRESENT CONCRETE	27
COMPOSITE MODEL ANALYSIS USING ADINA	27
FURTHER STUDIES USING COMPOSITE MODELS	28
CONCRETE MATERIAL MODEL PROGRAM SINGER	29

CONTENTS continued

	Page
ANALYSIS OF BEAMS USING SINGER	32
ANALYSIS OF BEAM USING MARC	33
CONCLUSIONS	34
RECOMMENDATION	35
REFERENCES	35

BACKGROUND

OPNAVINST 8023.2A assigns NAVFAC the responsibility to develop standards, criteria, instructions, and manuals needed to plan and design facilities related to explosives operations, and to sponsor appropriate engineering investigations and research. Certain structural performance criteria, intended to protect people and property from sources of potential explosives, require upgrading to fully utilize the inherent performance capability of the structure.

This work effort is directed toward improving techniques for predicting the dynamic response and behavior of reinforced concrete slabs that are a basic structural element in blast resistant construction. The safety and cost of ordnance facilities depends heavily on the accuracy of methods for predicting the structural response. Finite element technology, although perhaps complex in its applications, has greatly improved the accuracy of structural computations, allowing the computer to be utilized to analyze more refined (structural) mathematical models than could previously be done by hand computation.

A major problem in the use of computer analysis programs such as the various finite element programs is the characterization of the composite steel-concrete interaction in reinforced-concrete structural elements. This nonlinear behavior is very difficult to approximate and idealize to suit the various material description models in use. Of particular importance is the accurate representation of structural stiffness (a function of modulus of elasticity and moment of inertia) as a function of loading. The stiffness function is a prime factor that governs the deflection of the structural system. Most elements used to represent reinforced concrete attempt to represent the total composite behavior rather than the behavior of both reinforcing and concrete.

Under the action of external loads, a structural element is deformed causing internal forces in the element. The function of these internal forces is to resist the movement of the mass; hence the sum of the internal forces is defined as the resistance. The resistance of a structural element is a reactive force associated with the deflection of the element produced by the applied load. It is convenient to consider the resistance as an equivalent load in the same manner as the applied load, but opposite in direction. The variation of the resistance versus displacement is expressed by a resistance-deflection function and may be represented as in Figure 1.

Depending upon the magnitudes of the dynamic load and deflections permitted, one of three types of reinforced concrete cross sections can result: (1) Type I where the concrete cover over the reinforcement on both surfaces of the element remains intact, (2) Type II where the concrete cover over the compression reinforcement is crushed but still connected to the element, and (3) Type III where the concrete cover on both surfaces of the element is disengaged. All three cross sections are illustrated in Figure 2 (Reference 1).

Elements which are designed using the full cross section (Type I) usually are encountered in those structures or portions of structures designed to resist the blast output at the intermediate- and/or low-pressure design ranges. This type of cross section is utilized in elements with maximum deflections corresponding to support rotations less than 2 degrees. Type I elements may be reinforced on either one or both faces.

Elements which undergo support rotations greater than 2 degrees exhibit crushing of the concrete cover over the compression reinforcement (Type II). Type II sections, which sustain crushing of the concrete without any additional disengagement of the concrete cover, are encountered in structures at the intermediate- and low-pressure design ranges when the maximum deflections conform to support rotations greater than 2 degrees but less than 5 degrees. However, shear reinforcement is required.

Type III elements require special design. Sufficient compression reinforcement must be available to fully develop the tension steel

(tension and compression reinforcement must be equal), and lacing reinforcement must be present to prevent buckling of the compression steel and disengagement of the concrete between the layers of reinforcement. Elements of Type III design with lacing may undergo support rotations to 12 degrees.

It is of interest to examine the load characteristics of components of reinforced concrete. Figure 3 gives typical stress strain curves for reinforcing steel and Figure 4 gives a typical stress strain curve for concrete (Reference 2). Such observed behavior is the basis for developing material model representations for use in analysis.

YIELD-STRESS MOMENT AND MOMENT OF INERTIA

The initial yield moment of a reinforced-concrete cross section may be defined as the moment required for the steel in tension or the concrete in compression to just reach its yield limit. The reinforcement provided in actual construction must be governed by the former case; therefore, only the derivation for the under-reinforcement case (steel-in-tension yield) is described below, based on Reference 3.

A typical cross section of a reinforced-concrete section is shown in Figure 5, and the strain diagram is shown in Figure 6 where A_s and A'_s are the areas of the steel reinforcement in tension and compression, respectively. The strain level in tension steel is ϵ_t , in concrete is ϵ_c , and in compression steel is ϵ' . The strains are related by the following equations:

$$\frac{\epsilon_t}{\epsilon_c} = - \frac{d - Kd}{Kd} = - \frac{1 - K}{K}$$

$$\frac{\epsilon'}{\epsilon_c} = - \frac{d' - Kd}{Kd} = - \frac{\frac{d'}{d} - K}{K} \quad (1)$$

The stresses in steel are as follows:

$$\begin{aligned}\sigma_s &= -n\sigma_c \frac{1-K}{K} = \text{stress in tension steel} \\ \sigma'_s &= -n\sigma_c \frac{\frac{d'}{d} - K}{K} = \text{stress in compression steel}\end{aligned}\quad (2)$$

where $n = E_s/E_c$, the ratio of modulus of elasticity of steel to concrete.

Denoting the area of steel as a fraction of the area of the concrete section, i.e.,

$$\begin{aligned}p &= \frac{A_s}{bd} \\ p' &= \frac{A'_s}{bd}\end{aligned}\quad (3)$$

the equation of equilibrium becomes

$$\sigma_s A_s + \sigma'_s A'_s + \frac{1}{2} \sigma_c Kbd = 0 \quad (4)$$

This can be rewritten after some arrangement into the form

$$K^2 + 2(np + np')K - (2np + 2np' \frac{d'}{d}) = 0$$

Therefore the solution of K becomes

$$K = \sqrt{(2np + 2np' \frac{d'}{d}) + (np + np')^2} - (np + np') \quad (5)$$

The yield moment for the under reinforcement case is

$$M = \sigma_s A_s (d - \frac{Kd}{3}) + \sigma'_s A'_s (d' - \frac{Kd}{3})$$

or

$$M = A_s j d \sigma_s \quad (6)$$

where

$$j = 1 - \frac{K}{3} + \left(\frac{p'}{p}\right) \frac{\left(\frac{d'}{d} - K\right) \left(\frac{d'}{d} - \frac{K}{3}\right)}{1 - K} \quad (7)$$

If the solution of Equation 5 is such that $K > d'/d$, then the stress in compression steel is

$$\sigma'_s = 2n\sigma_c \frac{\frac{d'}{d} - K}{K} = 2 \frac{\frac{d'}{d} - K}{1 - K} \sigma_s \quad (8)$$

The equation of equilibrium for this case becomes

$$\sigma_s A_s + \sigma'_s A'_s + \frac{1}{2} \sigma_c Kbd - E_c \epsilon' A'_s = 0 \quad (9)$$

After some rearrangement, and the use of Equation 3, K becomes

$$K = \sqrt{2[np + (2n - 1)p' \frac{d'}{d}] + [np + (2n - 1)p']^2} - [np + (2n - 1)p'] \quad (10)$$

The form of Equation 6 remains the same except that for this case, j is defined as

$$j = 1 - \frac{K}{3} - \frac{(2n - 1)K - 2n \frac{d'}{d}}{n(1 - K)} \left(\frac{p'}{p}\right) \left(\frac{d'}{d} - \frac{K}{3}\right) \quad (11)$$

The transformed section moment of inertia is given by

$$I_c = \frac{1}{3} b Kd^3 + n A_s (d - Kd)^2 + (n - 1) A'_s (Kd - d')^2 \quad (12)$$

The value of I_c is the moment of inertia of the cracked concrete section of width b considering the compression concrete area and steel areas transformed into equivalent concrete areas and computed about the centroid of the transformed section. I_c may also be calculated from

$$I_c = F b d^3 \quad (13)$$

The coefficient F varies as the modular ratio n and the amount of reinforcement used. For sections with tension reinforcement only, the coefficient F is given in Figure 7. For other elements which are reinforced both in the compression and tension regions, the value of F cannot be obtained from any available design aids and, therefore, I_c must be calculated using the transformed section method as described in Equation 13 (Reference 1).

ULTIMATE STRENGTH MOMENT CAPACITY

The ultimate unit resisting moment M_u of a rectangular section of width b with tension reinforcement only is given by

$$M_u = A_s f_y \left(d - \frac{a}{2} \right) \quad (14)$$

where A_s = area of tension reinforcement, in.²

f_y = static design yield stress for reinforcement, psi

d = distance from extreme compression fiber to centroid of tension reinforcement, in.

a = depth of equivalent rectangular stress block = $A_s f_y / 0.85 b f'_c$; in.

b = width of compression face, in.

f'_c = static ultimate compressive strength of concrete, psi

The reinforcement ratio p is defined as

$$p = \frac{A_s}{bd} \quad (15)$$

To insure against sudden compression failures, the reinforcement ratio p must not exceed 0.75 of the ratio p_b which produces balanced conditions at ultimate strength and is given by

$$p_b = \frac{0.85 K_1 f'_c}{f_y} \left(\frac{87,000}{87,000 + f_y} \right) \quad (16)$$

where $K_1 = 0.85$ for f'_c up to 4,000 psi and is reduced 0.05 for each 1,000 psi in excess of 4,000 psi.

Figure 8 is a universal design chart giving the ultimate moment capacities of rectangular sections with tension reinforcement only for all values of p , f'_c , and f_y .

For a rectangular section of width b with compression reinforcement, the ultimate unit resisting moment is

$$M = (A_s - A'_s) f_y \left(d - \frac{a}{2} \right) + A'_s f_y (d - d') \quad (17)$$

where A'_s = area of compression reinforcement, in.²

d' = distance from extreme compression fiber centroid of compression reinforcement, in.

a = depth of equivalent rectangular stress block, in. = $(A_s - A'_s) f_y / 0.85 b f'_c$

The reinforcement ratio p' is

$$p' = \frac{A'_s}{bd} \quad (18)$$

Equation 17 is valid only when the compression steel reaches the value f_y at ultimate strength, and this condition is satisfied when

$$p - p' \geq 0.85 K_1 \frac{f'_c d'}{f_y d} \left(\frac{87,000}{87,000 - f_y} \right) \quad (19)$$

If $p - p'$ is less than the value given by Equation 19 or when compression steel is neglected, the calculated ultimate unit resisting moment should not exceed that given by Equation 14. The quantity $p - p'$ must not exceed 0.75 of the value of p_b given in Equation 16.

MODULUS OF ELASTICITY

The modulus of elasticity of concrete E_c may be computed by

$$E_c = w^{1.5} 33 \sqrt{f'_c} \text{ psi} \quad (20)$$

for values of w between 90 and 155 lb/ft³, where w is the unit weight of concrete and normally equal to 145 lb/ft³.

The modulus of elasticity of reinforcing steel E_s is

$$E_s = 29 (10^6) \text{ psi} \quad (21)$$

The modular ratio n is

$$n = \frac{E_s}{E_c} \quad (22)$$

and may be taken as the nearest whole number.

ACI CODE APPROACH FOR COMPUTING MOMENT OF INERTIA FOR DEFLECTION

Since finite element analysis techniques require a characterization of the stiffness of the structural element, it is important to review several approaches for estimating moment of inertia.

The ACI code (Reference 4) states that where deflections are to be computed, those which occur immediately on application of load shall be computed by the usual methods or formulas for elastic deflections. Deflections shall be computed taking the modulus of elasticity for concrete as specified in Equation 20 and taking the effective moment of inertia as follows.

$$I_c = \left(\frac{M_{cr}}{M_a} \right)^3 I_g + \left[1 - \left(\frac{M_{cr}}{M_a} \right)^3 \right] I_{cr} \leq I_g \quad (23)$$

where

$$M_{cr} = \frac{f_r I_g}{y_t} \quad (24)$$

and

$$f_r = 7.5 \sqrt{f'_c}$$

I_{cr} = moment of inertia of cracked section transformed to concrete

I_c = effective moment of inertia for computation of deflection

I_g = moment of inertia of gross concrete section about the centroidal axis, neglecting the reinforcement

M_a = maximum moment in member at stage for which deflection is being computed

M_{cr} = cracking moment

y_t = distance from centroidal axis of gross section, neglecting the reinforcement, to extreme fiber in tension

Special provisions are included for lightweight aggregate.

For continuous spans, the effective moment of inertia may be taken as the average of the values obtained from Equation 23 for the critical positive and negative moment sections.

EQUIVALENT MODULUS APPROACH FOR COMPUTING DEFLECTION

Another approach for stiffness evaluation is the equivalent modulus (Reference 3). Assume that the displacements in the reinforced concrete structure shown in Figure 9 are in the following form:

$$\begin{aligned} u(x,y,z) &= -\frac{\partial W(x)}{\partial x} z = -W'(x)z \\ v(x,y,z) &= 0 \\ w(x,y,z) &= W(x) \end{aligned} \quad (26)$$

and the strains:

$$\begin{aligned} \epsilon_{xx} &= -\frac{\partial^2 W(x)}{\partial x^2} z = -W''(x)z \\ \epsilon_{zz} &= \epsilon_{yy} = \epsilon_{xz} = \epsilon_{xy} = \epsilon_{yz} = 0 \end{aligned} \quad (27)$$

Assuming that the vertical stress $\sigma_{zz} = 0$

$$\begin{aligned} (\lambda + 2G) \epsilon_{zz} + \lambda(\epsilon_{xx} + \epsilon_{yy}) &= 0 \\ \epsilon_{zz} &= -\frac{\lambda}{\lambda + 2G} (\epsilon_{xx} + \epsilon_{yy}) = \frac{\lambda}{\lambda + 2G} W''(x)z \end{aligned} \quad (28)$$

and

$$\begin{aligned} \sigma_{xx} &= (\lambda + 2G) \epsilon_{xx} + \lambda \epsilon_{zz} = \left[(\lambda + 2G) - \frac{\lambda^2}{\lambda + 2G} \right] \epsilon_{xx} \\ &= \frac{E}{(1 - \nu^2)} \epsilon_{xx} = \frac{D}{I} \epsilon_{xx} = -\frac{D}{I} W''(x)z \end{aligned} \quad (29)$$

where

$$D = \frac{EI}{1 - \nu^2}$$

Now the moment M_x is given by

$$M_x = -b \int_{-h/2}^{h/2} \sigma_{xx} z \, dz \quad (30)$$

$$M_x = \frac{b D}{I} w''(x) \int_{-h/2}^{h/2} z^2 \, dz = D w''(x)$$

From the strain distribution, Figure 10

$$w''(x) = \frac{\epsilon_t}{(1 - k) d} \quad (31)$$

$$\epsilon_t = (1 - k) d w''(x)$$

Moment of the section is then given by

$$M = A_s j d \sigma_s = A_s j d E_s \epsilon_t \quad (32)$$

$$M = A_s j E_s (1 - k) d^2 w''(x) = D w''(x)$$

Also

$$D = A_s j E_s (1 - k) d^2 = \frac{EI}{(1 - \nu^2)} \quad (33)$$

Therefore the effective E for the concrete section is given by

$$E = \frac{A_s j E_s (1 - k) d^2 (1 - \nu^2)}{I} \quad (34)$$

where I is I_g .

NAVFAC P-397 APPROACH FOR COMPUTING MOMENT OF INERTIA FOR DEFLECTION

A third approach to stiffness is given in NAVFAC P-397 (Reference 1). The determination of the deflection of a reinforced concrete member in the elastic and elasto-plastic ranges is complicated by the fact that the effective moment of inertia of the cross section along the element changes continually as cracking progresses, and further by the fact that the modulus of elasticity changes as the stress increases. Reference 1 recommends that the computation of deflections use the average moment of inertia I_a

$$I_a = \frac{I_g + I_c}{2} \quad (35)$$

where I_g = moment of inertia of the gross concrete cross section of width b about its centroid (neglecting steel areas) and is equal to

$$I_g = \frac{bT^3}{12} \quad (36)$$

where I_c is the cracked moment of inertia from Equation 13. The modulus of elasticity shall be that of the concrete as defined by Equation 20.

MODEL REINFORCED CONCRETE BEAMS

To study strength-reduction direct models and their ability to reproduce prototype structural behavior, a series of model beam tests had been previously conducted (Reference 5). The model beams were selected from prototype beam tests conducted at the Portland Cement Association Laboratory (Reference 6) and the University of Illinois (Reference 7). Models were selected to reproduce tension failures,

compression failures, and shear failures. The beams were selected for this study because the number of test specimens of both model and prototype gave high reliability to the test results. This section will describe the experimental test results.

Tension Failures

A series of prototype beams was selected from which strength-reduction models were made (Figures 11 and 12). The strength-reduction models were able to reproduce the proper crack pattern and mode of failure. The average failure load of the model beams was 5% above the scaled prototype value. Typical deflection curves are shown in Figure 13.

Compression Failures

A model of a prototype beam (Reference 6) failing in compression was constructed in a procedure similar to the beams with tension failures. The length scale factor was set at 8 to permit reuse of the forms, and the strength scale factor was determined to be 3.7 based on the yield point of the model reinforcement (Figure 14). The results of the test (Figure 14) indicate ultimate loads approximately 9% higher than those scaled from the prototype. This in part may be caused by a minor modeling dissimilarity in the choice of reinforcing steel in the model (see Reference 5).

Shear Failures

The fourth set of strength-reduction models, consisting of two series of tests, attempted to reproduce shear failure. This series (Figure 15) was successful in reproducing a shear failure with loads approximately 7% higher than the scaled prototype values.

ANALYSIS BY EQUIVALENT BEAM

The objective of the analysis was to duplicate the load-deflection history observed in test data and to duplicate failure loading to determine ultimate resistance. The nonlinear finite element program ADINA (Reference 8) was used for this comparison. Beam elements were selected as the most direct technique to represent the test beams, using an elasto-plastic material model. The material model for elasto-plastic beams requires definition of a rectangular section, elastic modulus, Poisson's ratio, and yield stress. The decision was made to use the actual beam cross section dimension thus implicitly specifying a gross moment of inertia.

Tension Failure

There were three choices for determination of stiffness namely:

- (1) ACI approach using Equation 23, to determine effective I_c and concrete modulus
- (2) NAVFAC P-397 approach using Equation 35 to determine average I_a and concrete modulus and
- (3) Equation 34 to determine effective E and gross I .

The results of 1 and 3 (curve 1, Figure 16) were identical; however 2 gave a stiffness 1.28 times greater (curve 2, Figure 16). The program ADINA utilizes gross section moments of inertia and therefore adjusted moduli were input. Figure 16 shows a comparison between test data and computer solution. The conclusion in this case is that gross moment of inertia is effective only at very low loads (less than 10% of ultimate moment). The use of cracked moment of inertia is a better representation of behavior.

The program solution fails to achieve equilibrium at the point (A) of yielding. Use of the equilibrium check terminates the solution at this point. Omission of the equilibrium check allows continuation of the solution up until the point of solution instability. Further refinement of the time step allowed the problem to be solved with the equilibrium check active; results were the same as the preceding. Nonlinear solutions resemble dynamic problems in that small time steps are required to preserve equilibrium balance. However, no rule has been developed to guide in time step selection. Omission of equilibrium check resulted in solutions of acceptable accuracy in these problems.

Compression Failure

The cracked moment of inertia was used to estimate stiffness. Results are shown in Figure 17. As above the solution terminated prematurely when the equilibrium check was utilized with a 25 step solution. The solution without equilibrium check terminated with a stiffness matrix not being positive-definite at the point when a full plastic moment developed at mid-span indicating a failure mechanism. It is important to note that the finite element representation does not give any indication of the type of failure or stress condition in the actual beam. Thus it is necessary to analyze the actual section to determine its failure mode. Initial observation would be misleading and indicates a tension failure having large yield capacity. The actual failure was a sudden brittle compression failure.

Shear Failure

The cracked moment of inertia was used to estimate the stiffness. Results are shown in Figure 18. The stiffness in this analysis is greater than the actual. This is a limitation of an elasto-plastic model when the beam exhibits early nonlinearities. Although the initial stiffness is in agreement, the overall stiffness is about half that originally estimated based on a cracked section. This is attributed to

the shear mode of failure. The results of the analysis show that the shear stress of the cross section would be exceeded. However, the user must adjust the results since no internal failure mechanism exists for shear. The exact occurrence of the point of shear failure is unknown since the beam computationally "yields" rapidly between 400 and 405 lb and the exact failure shear stress is not known. The burden is placed upon the user to note shear failures since the solution will proceed. This is a critical limitation in cases of multicomponent structures since the solution would not be valid past the point of shear failure.

It is possible to utilize a displacement loading function rather than a force loading function. This could be accomplished by stiff springs at load points and reactions and a corresponding high force to induce displacement. The relative stiffness of the beam is small in comparison to the springs, and essentially adds no additional resistance. Thus deflections are induced to the beam and reactions computed to evaluate loading. This approach allows for load drop-off with increasing deflection beyond ultimate. Test procedures generally utilizing load machines induce displacement into the structure during loading. The result gives a reduction of load capacity beyond ultimate with the member continuing to deflect until collapse. Actual service conditions usually impose a constant loading. However, it is limited to simple loading conditions involving concentrated loads. This limits its usefulness. Figure 18 shows results including the drop-in load for the shear beam failure beyond failure.

Results indicate a more detailed analysis is required to properly evaluate the inelastic behavior beyond yielding.

MATERIAL MODELS FOR COMPOSITE REPRESENTATION OF REINFORCED CONCRETE

The previous section demonstrated that the use of beam elements was not totally satisfactory in predicting the mode of failure. A higher order of modeling utilizing an independent representation of concrete and reinforcement has potential for predicting failure mechanisms more realistically.

The direct modeling of concrete requires use of plastic material relationships. Various types of nonlinear material properties have been in use. The more common will be reviewed here.

Variable Modulus Model

This model is an attempt to provide for changes in the material strength parameters with volumetric strain history (Reference 9). The incremental stiffness parameters of bulk modulus K and shear modulus G , and unloading modulus are input as functions of volumetric strain. This allows for variation of Poisson's ratio with load. This model does not have a formal yield or failure criterion. Tensile limits may or may not be incorporated. As soon as the tensile stress at an integration point exceeds a reference stress the normal stiffness and shear stiffness across the failure plane are multiplied by reduction factors.

Tresca Yield Condition Maximum Shear Theory

This condition asserts that yielding occurs when the maximum shear stress reaches the prescribed value C_Y (Reference 10). Mathematically, the condition is expressed in its simplest form when given in terms of principal stresses. Thus for $\sigma_I > \sigma_{II} > \sigma_{III}$, the Tresca yield condition is given as

$$\frac{1}{2}(\sigma_I - \sigma_{III}) = C_Y \quad (\text{a constant}) \quad (37)$$

To relate the yield constant C_Y to the yield stress in simple tension σ_Y , the maximum shear in simple tension at yielding is observed (by Mohr's circles of Figure 19a, for example) to be $\sigma_Y/2$. Therefore when referred to the yield stress in simple tension, Tresca's yield condition becomes

$$\sigma_I - \sigma_{III} = \sigma_Y \quad (38)$$

The yield point for a state of stress that is so-called "pure shear" may also be used as a reference stress in establishing the yield constant C_Y . Thus if the pure shear yield point value is k , the yield constant C_Y equals k (again the Mohr's circles clearly show this result, as in Figure 19b), and the Tresca yield criterion is written in the form

$$\sigma_I - \sigma_{III} = 2k \quad (39)$$

For the biaxial state of stress, Figure 20 shows the stress condition. In this case $\sigma_{II} = 0$. The Tresca yield condition is the linear segments. The von Mises' yield condition is shown by the ellipse. This will be discussed in the next section.

Von Mises' Yield Condition (Distortion Energy Theory)

This condition asserts that yielding occurs when the second deviator stress invariant attains a specified value (Reference 10). Mathematically, the von Mises' yield condition states

$$(\sigma_I - \sigma_{II})^2 + (\sigma_{II} - \sigma_{III})^2 + (\sigma_{III} - \sigma_I)^2 = 6C_Y^2 \quad (40)$$

With reference to the yield stress in simple tension, it is easily shown that Equation 40 becomes

$$(\sigma_I - \sigma_{II})^2 + (\sigma_{II} - \sigma_{III})^2 + (\sigma_{III} - \sigma_I)^2 = 2\sigma_Y^2 \quad (41)$$

Also, with respect to the pure shear yield value k , von Mises' condition Equation 40 appears in the form

$$(\sigma_I - \sigma_{II})^2 + (\sigma_{II} - \sigma_{III})^2 + (\sigma_{III} - \sigma_I)^2 = 6k^2 \quad (42)$$

For a biaxial state of stress the von Mises' yield condition becomes

$$\sigma_I^2 - \sigma_I \sigma_{III} + \sigma_{III}^2 = \sigma_y^2 \quad (43)$$

which is the ellipse

$$\left(\frac{\sigma_I}{\sigma_y}\right)^2 - \frac{\sigma_I \sigma_{III}}{\sigma_y^2} + \left(\frac{\sigma_{III}}{\sigma_y}\right)^2 = 1 \quad (44)$$

The von Mises' model is specified in terms of Young's modulus, Poisson's ratio, yield stress, and strain hardening modulus. Two variations of hardening may occur--isotropic and kinematic hardening.

A stress space is established by using stress magnitude as the measure of distance along the coordinate axes. In the Haigh-Westergaard stress space of Figure 21 the coordinate axes are associated with the principal stresses. Every point in this space corresponds to a state of stress, and the position vector of any such point $P(\sigma_I, \sigma_{II}, \sigma_{III})$ may be resolved into a component OA along the line OZ , which makes equal angles with the coordinate axes, and a component OB in the plane (known as the II-plane) which is perpendicular to OZ and passes through the origin. The component along OZ , for which $\sigma_I = \sigma_{II} = \sigma_{III}$, represents hydrostatic stress, so that the component in the II-plane represents the deviator portion of the stress state. It is shown that the equation of the II-plane is given by

$$\sigma_I + \sigma_{II} + \sigma_{III} = 0 \quad (45)$$

In stress space, the yield condition $f_2(\sigma_I, \sigma_{II}, \sigma_{III}) = C_Y$, defines the so-called yield surface. Since the yield conditions are independent of hydrostatic stress, such yield surfaces are general cylinders having their generators parallel to OZ. Stress points that lie inside the cylindrical yield surface represent elastic stress states, those which lie on the yield surface represent incipient plastic stress states. The intersection of the yield surface with the II-plane is called the yield curve.

In a true view of the II-plane, looking along OZ toward the origin O, the principal stress axes appear symmetrically placed 120° apart as shown in Figure 22a. The yield curves for the Tresca and von Mises' yield conditions appear in the II-plane as shown in Figure 22b and c. In Figure 22b, these curves are drawn with reference to Equations 37 and 40 using the yield stress in simple tension as the basis. For this situation, the von Mises' circle of radius $\sqrt{2/3} \sigma_Y$ is seen to circumscribe the regular Tresca hexagon. In Figure 22c, the two yield curves are based upon the yield stress k in pure shear. Here the von Mises' circle is inscribed in the Tresca hexagon.

The assumption of isotropic hardening under loading conditions postulates that the yield surface simply increases in size and maintains its original shape. Thus in the II-plane the yield curves for von Mises' and Tresca conditions are the concentric circles and regular hexagons.

Continued loading after initial yield is reached leads to plastic deformation which may be accompanied by changes in the yield surface. For an assumed perfectly plastic material, the yield surface does not change during plastic deformation and the initial yield condition remains valid. This corresponds to the one-dimensional perfectly plastic case (isotropic). For a strain hardening material, however, plastic deformation is generally accompanied by changes in the yield surface. To

account for such changes it is necessary that the yield function $f_1(\sigma_{ij}) = 0$ be generalized to define subsequent yield surfaces beyond the initial one. A generalization is effected by introduction of the loading function

$$f_1^*(\sigma_{ij}, \varepsilon_{ij}^P, K) = 0 \quad (46)$$

which depends not only upon the stresses, but also upon the plastic strains ε_{ij}^P and the work-hardening characteristics represented by the parameter K . Equation 46 defines a loading surface in the sense that $f_1^* = 0$ is the yield surface, $f_1^* < 0$ is a surface in the (elastic) region inside the yield surface and $f_1^* > 0$, being outside the yield surface, has no meaning.

In kinematic hardening, the initial yield surface is translated to a new location in stress space without change in size or shape. Thus a yield constant defining an initial yield surface is replaced by

$$f_1(\sigma_{ij} - \alpha_{ij}) = 0 \quad (47)$$

where the α_{ij} are coordinates of the center of the new yield surface. If linear hardening is assumed,

$$\dot{\alpha}_{ij} = c \dot{\varepsilon}_{ij}^P \quad (48)$$

where c is a constant.

Drucker-Prager Model

It is convenient to derive relationships which are based upon terms that are independent of axis orientation. There are functions of the stress or strain tensors which have the same definition regardless of the coordinate system in which they are defined. They are called the stress or strain "invariants" (Reference 9). The stress invariants may be defined as:

$$J_1 = \sigma_{ii} = \sigma_{xx} + \sigma_{yy} + \sigma_{zz} \quad (49)$$

$$\begin{aligned} J_2 &= \frac{1}{2} [\sigma_{ii} \sigma_{jj} - \sigma_{ij} \sigma_{ji}] \\ &= \sigma_{xx} \sigma_{yy} + \sigma_{yy} \sigma_{zz} + \sigma_{zz} \sigma_{xx} - \sigma_{xy}^2 - \sigma_{yz}^2 - \sigma_{zx}^2 \end{aligned} \quad (50)$$

where J_1 and J_2 are defined as the first and second stress invariant respectively. The first invariant of the stress tensor J_1 equals three times the average hydrostatic stress or pressure. The first invariant is generally used in constitutive relationships to introduce the influence of volumetric or hydrostatic effects. The shearing, or deviatoric portion of the stress or strain tensor is referred to as the deviatoric. The invariants of the deviatoric are distinguished by primes. The first invariant of the stress deviatoric, $J'_1 = 0$ indicating the absence of volumetric effects. The second invariant of the stress deviatoric, J'_2 , is defined as:

$$\begin{aligned} J'_2 &= \frac{1}{6} [(\sigma_{xx} - \sigma_{yy})^2 + (\sigma_{yy} - \sigma_{zz})^2 + (\sigma_{zz} - \sigma_{xx})^2] \\ &\quad + \sigma_{xy}^2 + \sigma_{yz}^2 + \sigma_{zx}^2 \end{aligned} \quad (51)$$

This is a function of the maximum shearing stresses. It is also related to the shear stress acting on the octahedral plane which is the plane perpendicular to a line equidistant from the 3 major axes in principle stress space. The normal and shear stresses acting on this plane are defined as:

$$\begin{aligned}\sigma_{\text{oct}} &= \frac{1}{3} \sigma_{ii} = p \\ \tau_{\text{oct}} &= \frac{1}{3} \sqrt{(\sigma_{11} - \sigma_{22})^2 + (\sigma_{22} - \sigma_{33})^2 + (\sigma_{33} - \sigma_{11})^2}\end{aligned}\tag{52}$$

The second invariant of the deviatoric is generally used to provide an axis-independent means of introducing the influence of shearing behavior.

Once plastic deformation is initiated, the constitutive equations of elasticity are no longer valid. Because plastic strains depend upon the entire loading history of the material, plastic stress-strain relations very often are given in terms of strain increments - the so-called incremental theories. By neglecting the elastic portion and by assuming that the principal axes of strain increment coincide with the principal stress axes, the Levy-Mises equations relate the total strain increments to the deviatoric stress components through the equations

$$d\epsilon_{ij} = s_{ij} d\lambda\tag{53}$$

Here the proportionality factor $d\lambda$ appears in differential form to emphasize that incremental strains are being related to finite stress components. The factor $d\lambda$ may change during loading and is therefore a scalar multiplier and not a fixed constant. Equation 53 represents the flow rule for a rigid-perfectly plastic material.

If the strain increment is split into elastic and plastic portions according to

$$d\epsilon_{ij} = d\epsilon_{ij}^E + d\epsilon_{ij}^P \quad (54)$$

and the plastic strain increments related to the stress deviator components by

$$d\epsilon_{ij}^P = s_{ij} d\lambda \quad (55)$$

the resulting equations are known as the Prandtl-Reuss equations. Equation 55 represents the flow rule for an elastic-perfectly plastic material. They provide a relationship between the plastic strain increments and the current stress deviators but do not specify the strain increment magnitudes.

The theories of plasticity utilized are generally limited to isotropic incremental flow theories for isotropic time-independent materials subjected to small strains under isothermal conditions (Reference 9). Yielding is generally defined to occur at some experimentally observed stress state. For example, a von Mises yield condition limits the square root of the second invariant of the stress deviatoric to some constant value, A.

$$\sqrt{J_2'} = A \quad (56)$$

For the Drucker-Prager yield condition the maximum shear stress is related to some function of the volumetric stress,

$$\sqrt{J_2'} = A + \alpha J_1 \quad (57)$$

where A and α are constants and the square root of J_2' is generally used to maintain units of stress. For the uniaxial strain or the triaxial shear test,

$$\sqrt{J_2'} = \frac{1}{\sqrt{3}}(\sigma_1 - \sigma_3) \text{ and } J_1 = 3P = \sigma_1 + 2\sigma_3 \quad (58)$$

The square root of the second invariant of the stress deviatoric, J_2' , may be plotted against P (equal to one-third the value of the first stress invariant, J_1) in order to evaluate A and α .

A straight line approximation for A and α in terms of cohesion, c , and friction angle, ϕ , from a Mohr-Coulomb diagram, are:

$$A = \frac{6c \cos \phi}{\sqrt{3} (3 - \sin \phi)} \quad \alpha = \frac{2 \sin \phi}{\sqrt{3} (3 - \sin \phi)} \quad (59)$$

On an incremental basis the flow rule may be specified as:

$$\dot{\epsilon}_{ij}^P = \lambda \frac{\partial \Phi}{\partial \sigma_{ij}} \quad (60)$$

The dot denotes an incremental relationship. The λ represents a non-negative scalar factor of proportionality (Reference 9). It is not a characteristic constant of the material. It is an arbitrary factor relating the energy dissipated in plastic flow to the work done by the external load. The Φ is the plastic potential function. When Φ is identical to the yield condition, for example in the Drucker-Prager failure theory, then:

$$\Phi = \sqrt{J_2'} - A - \alpha J_1 = 0 \quad (61)$$

and the flow rule is called "associated." Otherwise it is a non-associated flow rule (Reference 9).

Figure 23 shows the Drucker-Prager material model. Murtha and Crawford (Reference 11) demonstrate that A and α can be computed directly for concrete. This means all of the measured data is included in the

calculation of A and α and that no dependence on parameters c and ϕ is necessary. This is accomplished by computing J_1 and J_2' at intervals of 0.2 along the σ_1/f'_c axis. Values of σ_i/f'_c ($i = 1, 2, 3$) were computed for various points on the curves and from these values J_1 and J_2' were computed. The results are shown in Figure 24 where $A = 0.48 f'_c$ and $\alpha = 0.09$. In effect, Figure 24 demonstrates that the Drucker-Prager Model matches the envelopes of concrete in the compression quadrant.

Using Equation 59 to derive an equivalent ϕ and c gives $\phi = 12.5^\circ$ and $c = 0.395 f'_c$.

Mohr-Coulomb

The generalized Mohr-Coulomb behavior may be used to produce the following failure law for compression-compression zone.

$$3J_2 + \sqrt{3} \beta \sigma J_1 + \alpha J_1^2 = \sigma^2$$

where β , σ and σ_0 are material constants. For biaxial stress Kupfer (References 11 and 12) evaluated these constants as

$$\beta = \sqrt{3} \quad ; \quad \alpha = 1/5 \quad ; \quad \sigma = f'_c/3$$

In the tension-compression zone and tension-tension zones, failure may be defined by a series of straight lines based on the tensile strength of concrete.

ADINA Concrete Model

The failure criterion for this model is based on experimental data. Figure 25a and b show the form of input used to define this model. The basis for the model is the triaxial representation of experimental data (Reference 8) expressed in variable modulus format.

Unlike the Mohr-Coulomb or the Drucker-Prager plasticity models, once the stress state has reached its specific crushing point (ϵ_c , Figure 25), the stiffness of the material in all directions is reduced and all stresses are released. This model also allows a gradual reduction of stiffness with increasing stress.

CONCRETE BEHAVIOR

References 2, 12, 13, 14, 15, and 16 discuss concrete material properties. Figures 26 and 27 show the biaxial strength of concrete. It is obvious that the tensile strength is significantly weaker than the compressive strength. Figure 28 shows uniaxial and biaxial and lateral strain from two sources that are in general agreement. Figure 29 shows triaxial test data in compression. Figure 30 gives triaxial concrete strength for ratios of stress. This information is utilized in the ADINA concrete model.

MATERIAL MODELS AVAILABLE IN ADINA TO REPRESENT CONCRETE

Figures 31 and 32 show the material models available in ADINA possible for use in modeling concrete. As can be seen from the preceding discussion, a tension cutoff is essential to attempt to define failure of an element; only the variable modulus model and the concrete model incorporate this feature. Both the Drucker-Prager and von Mises models may satisfactorily represent the model in compression; however, they lack definition in the tensile region.

COMPOSITE MODEL ANALYSIS USING ADINA

A finite element model was prepared in which the concrete was represented by 2-dimensional quadrilateral elements and the reinforcement by truss elements. The steel reinforcement was modeled using the

elasto-plastic model. The concrete was modeled both by the ADINA Concrete Model and in another separate solution by the Variable Modulus Model. Results for the compression failure are shown in Figure 33. The concrete model was quite successful and predicted concrete crushing in the central compressive region. This run was quite satisfactory. The variable modulus model results did not indicate compression failure; thus its results, although capable of tracking the load deflection behavior, do not give an insight into failure. Further the material parameters are more suited toward soil mechanics analysis than reinforced concrete analysis.

Figure 34 shows the load deflection curve for an analysis of model beam 3 which failed in shear using the concrete model in ADINA. Agreement is very good. The model exhibited considerable cracking. Final failure was caused by concrete crushing. The interpretation or designation of a shear failure is not made by the program, although it is possible to reconstruct a failure mechanism from the description of cracking and crushing. Further work using ADINA utilized the concrete model since it best represented concrete behavior.

FURTHER STUDIES USING COMPOSITE MODELS

Two beams were selected from Reference 7 for which there were load deflection data. Both beams were identical except that one beam had stirrups, the other had none. As before, using ADINA, reinforcement was modeled using truss elements. In this case this included both the longitudinal reinforcement as well as the stirrups. Figure 35 shows the results. Curve A shows results using the default value of the parameter for shear stiffness reduction of 0.5. Curve B shows results of reducing the shear stiffness reduction parameter equal to 0.01. Variations were made in the ADINA Concrete Model parameter Alpha (unloading ratio) but were found to have no effect on the solution, Curve A.

Figure 36 shows the results for the beam with stirrups. The parameters used in this example were the same as those used for Curve A of Figure 35. It may be seen that both Curve A, Figure 35, and Figure 36 give excellent agreement with the loading path of both beams. The results suggest stirrups can be modeled using truss elements with the ability to reproduce stiffness behavior. However, both examples display significantly more ductility than was observed in the actual beams. The absence of a failure mode cutoff in shear as discussed above can give results which grossly overestimate ductility. This is extremely important in estimating the dynamic response of structures. Variations were made in concrete failure strain and although these varied the load path, it did not alter the excessive ductility problem.

Figure 37 describes a beam-column with results of direct model (Reference 5) and prototype tests (Reference 6). The test specimens were modeled for finite element analysis in a similar way to previously described work. This study case is intended to evaluate the thrust-moment interaction failure mode. As a failure mode, it is a difficult test of the finite element procedure since it depends directly on the ability of the program to define a failure condition. Results are given in Figure 38. The initial results without equilibrium check overestimate failure thrust-moment. Use of stiff spring techniques for loading did not improve results. With the equilibrium - condition - check active results approached the range of acceptable solution as the load increment was reduced. The results indicate that it is possible to obtain a good approximation of failure thrust-moment however, the user must insure sufficiently small load steps to preserve equilibrium balance.

CONCRETE MATERIAL MODEL PROGRAM SINGER

Program SINGER (Reference 17) is a finite element program which is formulated to solve for equilibrium by the minimization of the work function. The program is intended for reinforced concrete 2D elements simulating the actual nonlinear behavior including crushing, spalling,

etc., under both static and dynamic loads. Dynamic loads are treated by time step solution at selected points in time. The state of the system is defined by the work function which contains all of the forces acting on the system. The reinforced concrete beam-column is represented by a gross element model (a one-dimensional idealization). Axial and flexural deformations are modeled explicitly. Inelastic deformations are modeled up to element failure. The coupling of axial and flexural distortions is represented by nonlinear terms in the strain-displacement relation. Also included is the variability of neutral axis. The constitutive laws model the behavior of concrete, both confined and unconfined, and reinforcing steel.

The numerical energy evaluation is based on the discretization of the energy stored in the element. It involves two principal tasks:

1. The computation of the internal-energy density at a discrete number of points in the element.
2. The integration of the internal-energy density over the volume of the element.

The computation of the internal-energy density during the solution process of a typical time step, from t_1 to t_2 , is described with the aid of Figure 35. The term t_1 corresponds to the time at which the last equilibrium state of the system has been obtained, and t_2 denotes the time at which the next equilibrium state is sought. The stress-strain curves in Figure 35 govern the behavior of a discrete point of the element. The terms ϵ_1 and ϵ_2 denote strains at t_1 and t_2 , respectively; both loading ($\epsilon_2 > \epsilon_1$) and unloading ($\epsilon_2 < \epsilon_1$) cases are illustrated. The internal-energy density at time t_2 is

$$U_2^* = U_1^* + U_{12}^* \quad (63)$$

where

$$U_1^* = \int_0^{\epsilon_1} \sigma d\epsilon$$

represents the internal-energy density at t_1 , and

$$U_{12}^* = \int_{\epsilon_1}^{\epsilon_2} \sigma d\epsilon = \begin{cases} >0 & \text{if } \epsilon_2 > \epsilon_1 \\ <0 & \text{if } \epsilon_2 < \epsilon_1 \end{cases} \quad (64)$$

represents the change in the internal-energy density during the time step t_1, t_2 . It follows from Figure 39 that for a given value of strain ϵ_2 , there corresponds a unique value of stress. Consequently, the internal-energy density, and hence the internal energy, is uniquely defined by the strain state, which in turn is a unique function of the displacement state. Hence, in the neighborhood of an equilibrium state, the internal energy of the system is a unique function of the generalized coordinates. This is a major difference between this model and other models. The formulation by the energy approach allows for negative moduli values not possible in stiffness formulation methods. Consequently, the material stress-strain model in Figure 40 may be used to represent concrete past ultimate loading. A distinction is made between confined concrete and unconfined concrete. Figure 41 shows the results of rectangular prisms under concentrated load. The line represents values for use in flexure; p'' is the ratio of volume of lateral reinforcement to the volume of confined concrete; f_y'' is the reinforcement yield stress. The possible SINGER failure criteria considered are given here:

1. Flexural Failure

- a. Concrete Crushing
- b. Steel Fracture
- c. Bar Buckling and Concrete Crushing Simultaneously

2. Shear-Flexure Failure

- a. Detection of the Principal Diagonal Crack Leading to Failure
- b. Detection of the Principal Diagonal Crack Plus Yielding of the Web Reinforcement Leading to Failure

3. Axial Force Failure

- a. Concrete Crushing: 1a failure criteria applies
- b. Steel Fracture: 1b failure criteria applies
- c. Bar Buckling and Concrete Crushing Simultaneously:
1c failure criteria applies

ANALYSIS OF BEAMS USING SINGER

The compression failure and shear failure beams were studied using Program SINGER. Figure 43 shows the load-deflection diagram for the compression failure case. The program gives a reasonable approximation of the resistance function. However, the solution did not terminate with the failure of the member. The printed output gives a description of concrete crushing, cracking, and yielding indicating compression failure. This is extremely useful in interpreting beam behavior.

A major disadvantage of this program is its high cost, approximately six times the ADINA runs. The program thus is limited to those problems where the detailed modeling of reinforcement, stirrups confined and unconfined concrete is essential.

The shear failure beam was also analyzed using SINGER. Figure 43 gives the load deflection diagram. Results are quite good. The deflection increased rapidly at the failure load and the printed output indicated a diagonal tension failure.

The preceding examples demonstrate the capability of the SINGER composite model to accurately represent the load deflection of reinforced concrete elements. The only technical limitation is that the solution process does not terminate at failure but rather continues indicating large deflection (excessive ductility). This may be a limitation with multi-component structures in evaluating actual load carrying capacity and ductility.

ANALYSIS OF BEAM USING MARC

Program MARC is a nonlinear finite element program. The program contains a wide assortment of element types and to simplify input, mesh generators are available. The format for the program is very general, being keyed by word descriptors. An interesting feature of this program is that there is a 2D and 3D reinforcement element which is capable of being used with 2D plane strain elements and 3D plane strain elements. The element is described as a hollow element which contains reinforcing bars in an arbitrary orientation. The reinforcing bar element overlays the concrete element allowing for a generalized placement of reinforcing much less dependent on mesh configuration. Unfortunately serious limitations presently exist in the code. Nonlinear elasticity material models are limited to von Mises and Mohr-Coulomb. A concrete model is available for axisymmetric and shell analysis. Unfortunately, only one type of material model may be used in any problem. This thus restricts reinforcement behavior when used in conjunction with the concrete model. Present usage of this code requires payment of a royalty; thus costs of usage are more than double those by ADINA.

Several variations of the shear beam were prepared. Cracking is essential to the solution of this problem. This restricts the choice of elements to the axisymmetric 8-node quad. A large radius was used to consider an essentially plane problem. The reinforcement must follow the same material model as the concrete; this is clearly a limitation. Results are shown in Figure 44.

CONCLUSIONS

The following conclusions from the study are made:

1. Cracked moment of inertia and concrete modulus best represent the stiffness of a concrete section modeled by beam elements. This has an advantage over modified modulus techniques, particularly when axial load is included.
2. Use of beam elements may not represent shear and compression failure modes. The user must check for these failures.
3. Composite steel/concrete modeling techniques can be used successfully to model tension, shear and compression failure modes, however, the user must carefully analyze results.
4. The ADINA Concrete Model produces excellent agreement in tracking load deflection behavior and is recommended over the others.
5. The composite model may overestimate the ductility of reinforced concrete when shear and compression failures occur. Care must be taken to ensure sufficiently small load increments.
6. Nonlinear problems, like dynamic problems, require a small time step to preserve equilibrium balance.
7. Program SINGER has the capability for detailed modeling using beam element representation. This program is capable of providing insight into failure modes. However, it is relatively costly to use.
8. Program MARC does not appear to have any advantage over ADINA.

RECOMMENDATION

Further work is recommended in defining failure in terms of ductility, mode of behavior and reduction in load capacity. The functional utility of the structural member must be quantified in the post ultimate load range.

REFERENCES

1. Naval Facilities Engineering Command. NAVFAC P-397. Design of Structures to Resist Accidental Explosions. Washington, D.C., 1969.
2. Air Force Weapons Laboratory. AFWL TR 76-130: Behavior of Reinforced Concrete Beams Under Combined Axial and Lateral Load. Kirtland Air Force Base, N.M., May 1977.
3. Agbabian Associates. Dynamic Analysis of Magazine Headwalls in the Eskimo Tests for Department of Defense Explosives Safety Board, by D. P. Reddy. El Segundo, Calif., May 1976.
4. ACI Standard 318-71. Building Code Requirements for Reinforced Concrete. Detroit, Mich., Nov 1971.
5. Naval Civil Engineering Laboratory. Technical Report R-682: Concrete Model Analysis of Structural Elements Developing Strength Reduction Concepts, by J. M. Ferritto. Port Hueneme, Calif., May 1970.
6. E. Hognestad. "High Strength Bars as Concrete Reinforcement; Part 2 Control of Flexural Cracking." Portland Cement Association, Journal of the PCA Research and Development Laboratories, vol 4, no. 1, Jan 1962, pp 46-63.

7. K. G. Moody et al. Shear Strength of Reinforced Concrete Beams; Part 1, Tests of Simple Beams. American Concrete Institute Journal, Proceedings, vol 51, no. 4, Dec 1954, pp 317-332.
8. Massachusetts Institute of Technology. ADINA A Finite Element Program for Automatic Dynamic Incremental Nonlinear Analysis, by Klaus Jurgen Bathe. Cambridge, Mass., May 1977.
9. Civil Engineering Laboratory. Technical Note N-1324: Soil Mechanics and Advanced Computer Codes, by J. B. Forrest. Port Hueneme, Calif., Apr 1974.
10. George E. Mase. Continuum Mechanics. McGraw-Hill Company, New York, 1970.
11. Civil Engineering Laboratory. Technical Memorandum M-51-78-6: An Evaluation of Material Model Performance for Concrete Subject to Triaxial States of Compressive Stress, by R. N. Murtha and J. E. Crawford. Port Hueneme, Calif., Nov 1977.
12. Kupfer, H., Hilsdorf, H. K., and Rusch, H. Behavior of Concrete Under Biaxial Stresses, Journal of the American Concrete Institute, vol 66, no. 8, Aug 1969, pp 656-666.
13. Khan, M. H. and Saugy, B. Evaluation of the Influence of Some Concrete Characteristics on Nonlinear Behavior of a Prestressed Concrete Reactor Vessel, ACI publication, SP-34, Concrete for Nuclear Reactors, 1972.
14. Launay, P. and Gachon, H. Strain and Ultimate Strength of Concrete Under Triaxial Stress, ACI publication, SP-34, Concrete for Nuclear Reactors, 1972.

15. Air Force Weapons Laboratory. AFWL-TR-72-59 Vol I: Static Concrete Constitutive Relations Based on Cubical Specimens, by Endebrock, E. G. and Traina, L. A. Kirtland Air Force Base, N.M., Dec 1972.

16. Mills, L. L. and Zimmerman, R. M. "Compressive Strength of Plain Concrete Under Multiaxial Loading Conditions, ACI Journal, Proceedings, vol 67, no. 10, Oct 1970.

17. Air Force Weapons Laboratory. AFWL TR 74-228: SINGER: A Computer Code for General Analysis of Two Dimensional Concrete Structures, by R. J. Melosh et al. Kirtland Air Force Base, N.M., May 1975.

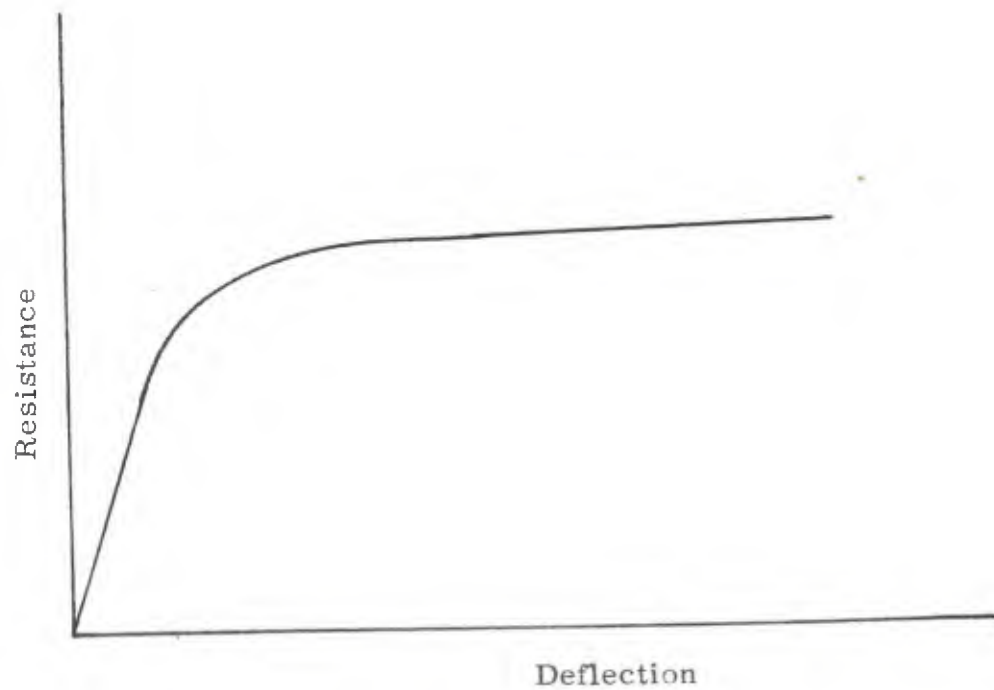
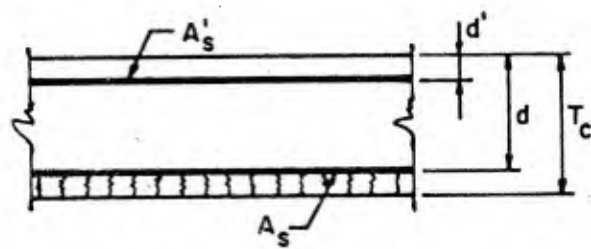
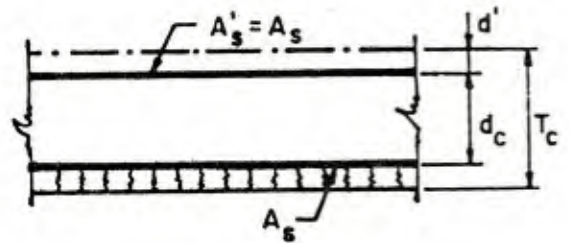


Figure 1. Typical resistance - deflection function.



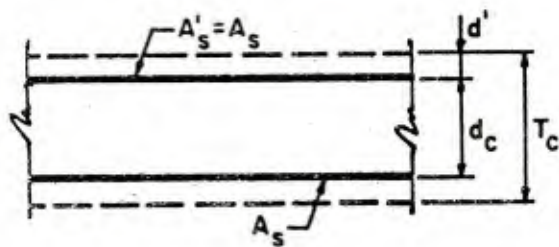
NO CRUSHING OR SPALLING

TYPE I



CRUSHING

TYPE II



SPALLING

TYPE III



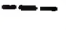
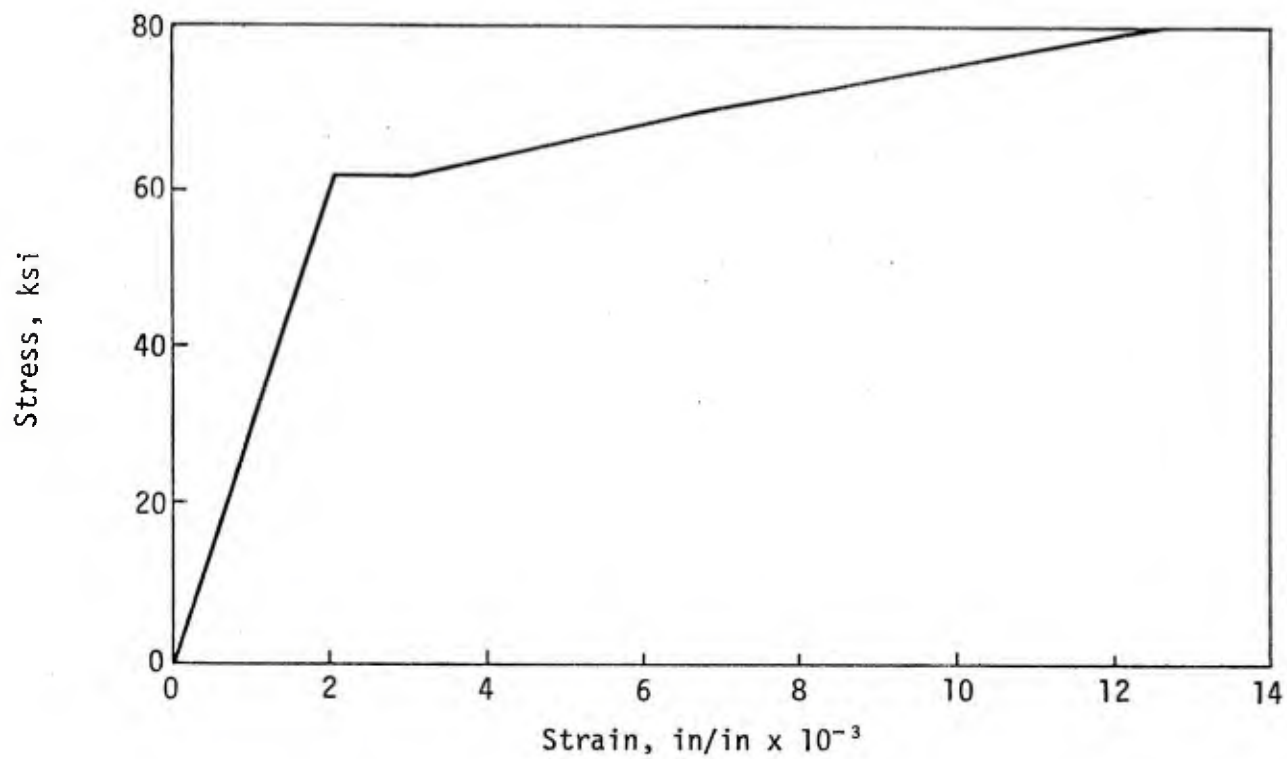
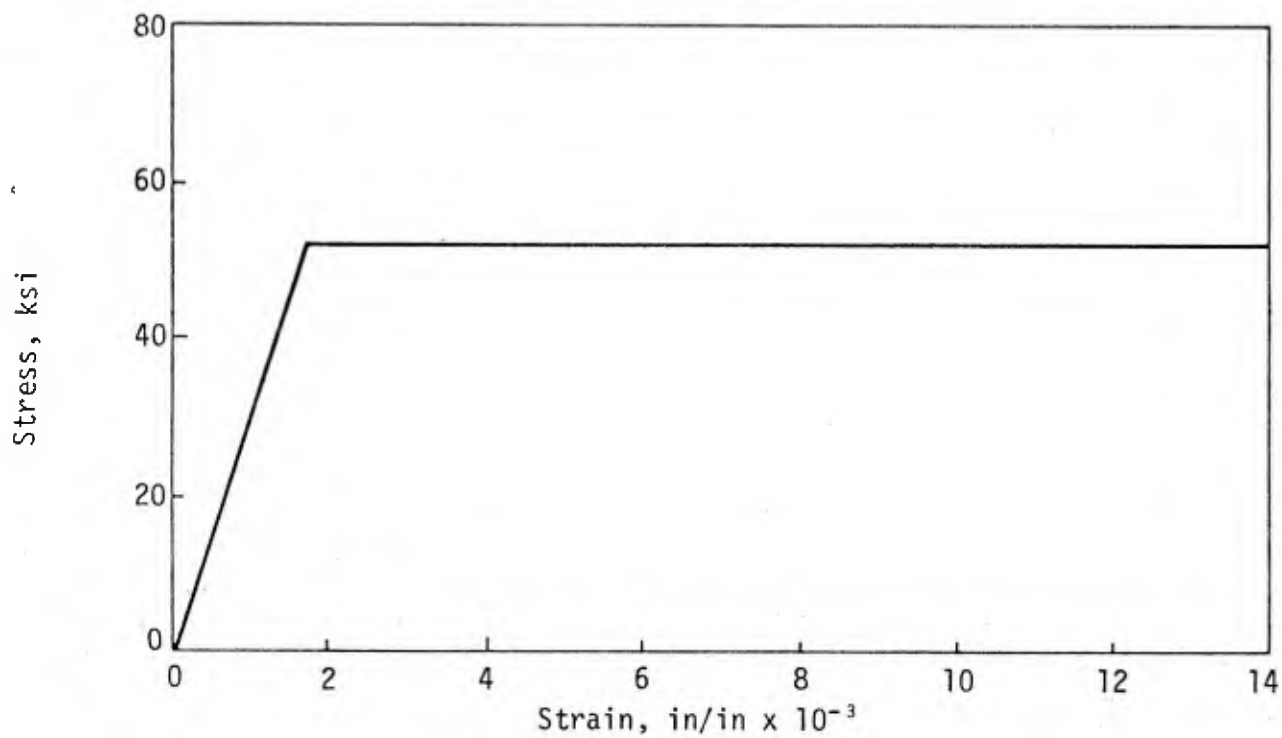
 CRACKING
 CRUSHING
 DISENGAGEMENT

Figure 2. Typical reinforced concrete cross sections.



(a) No. 6 Reinforcing Bar



(b) No. 2 Reinforcing Bar

Figure 3. Typical Stress-Strain Curves for Reinforcing Steel

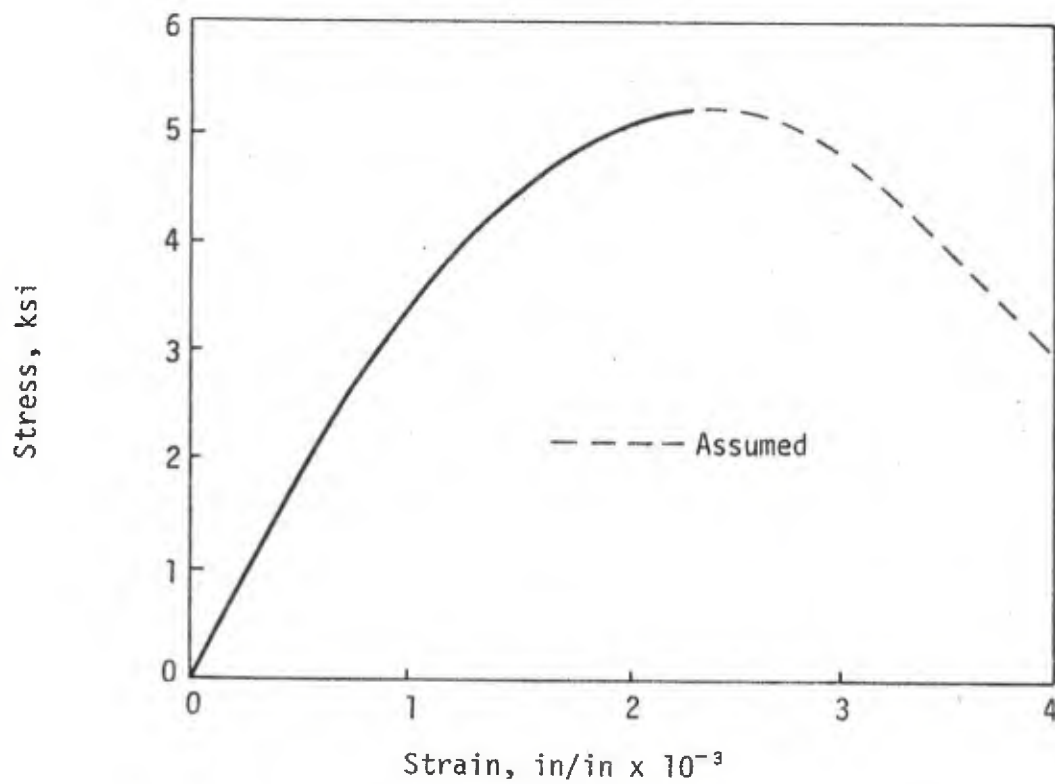


Figure 4. Typical Stress-Strain Curve for Concrete

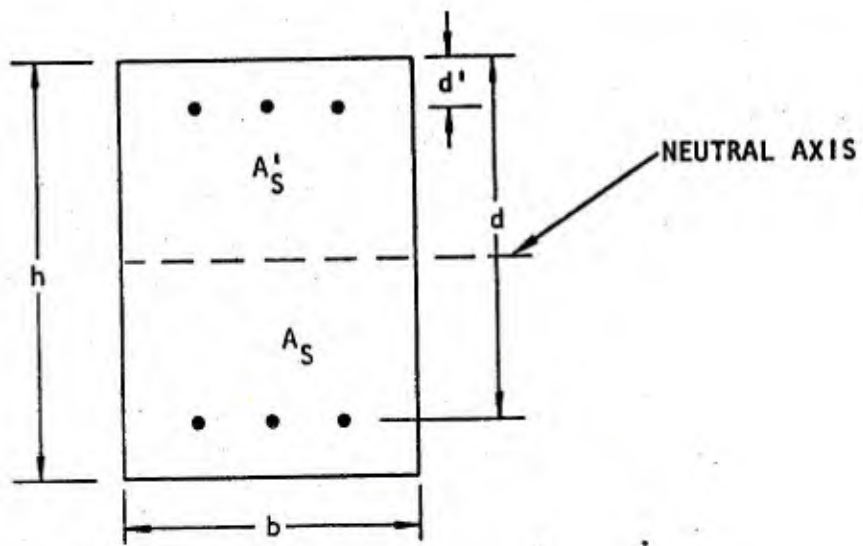


Figure 5. Reinforced concrete section.

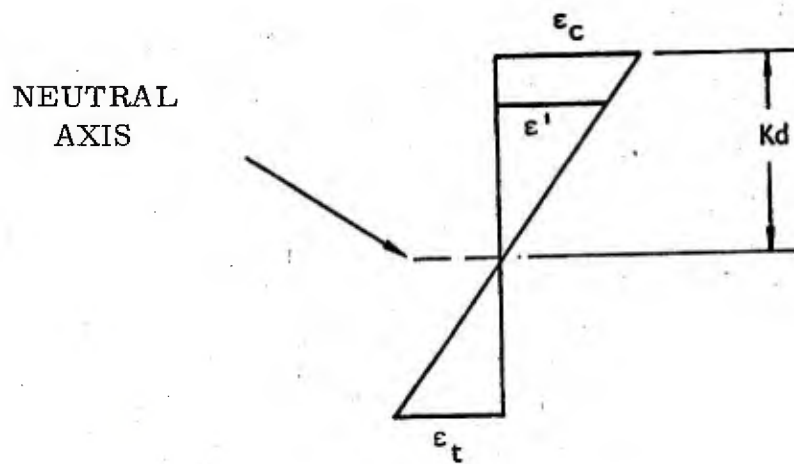


Figure6. Strain distribution across section.

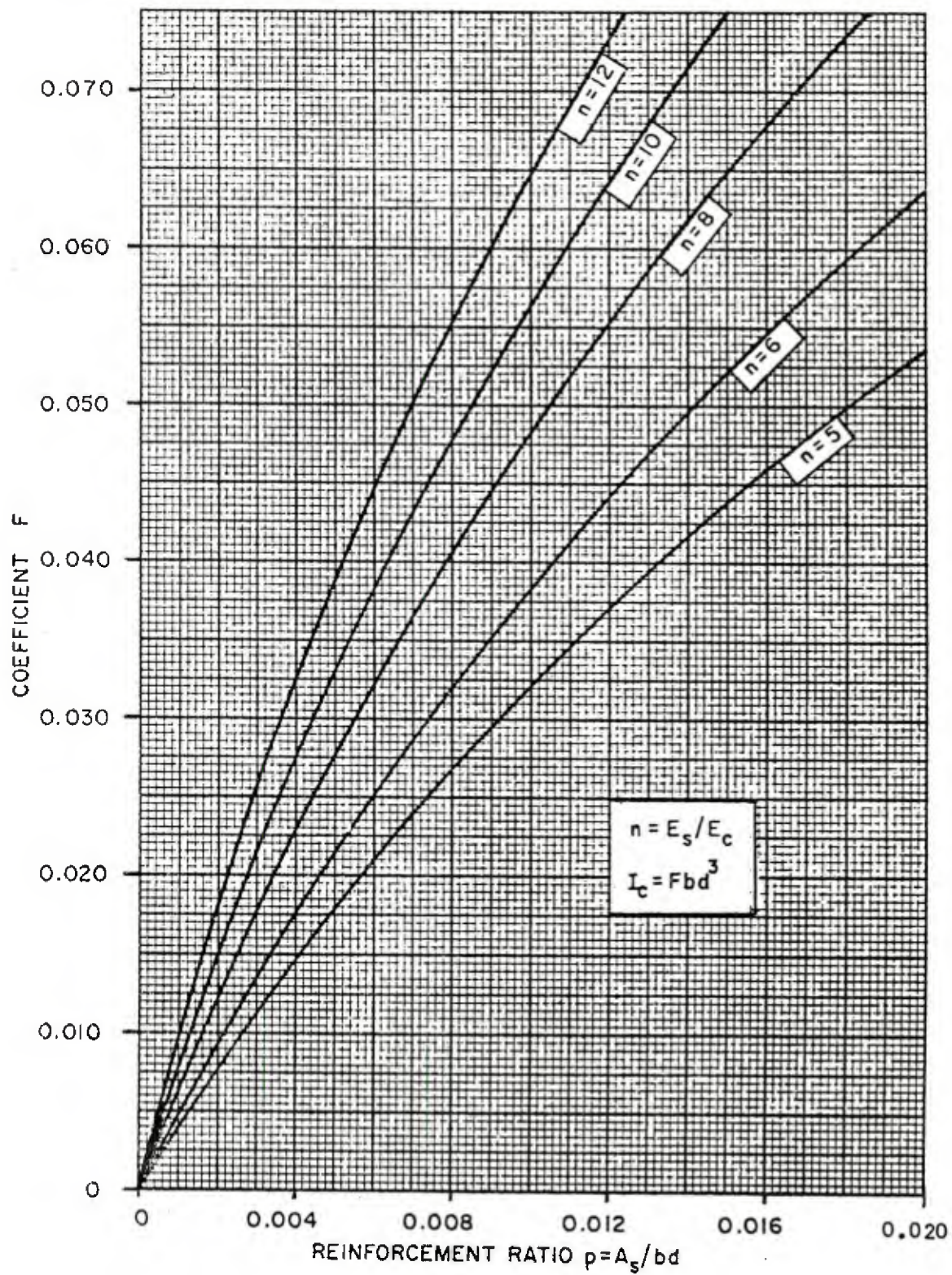


Figure 7. Coefficients for cracked moment of inertia.

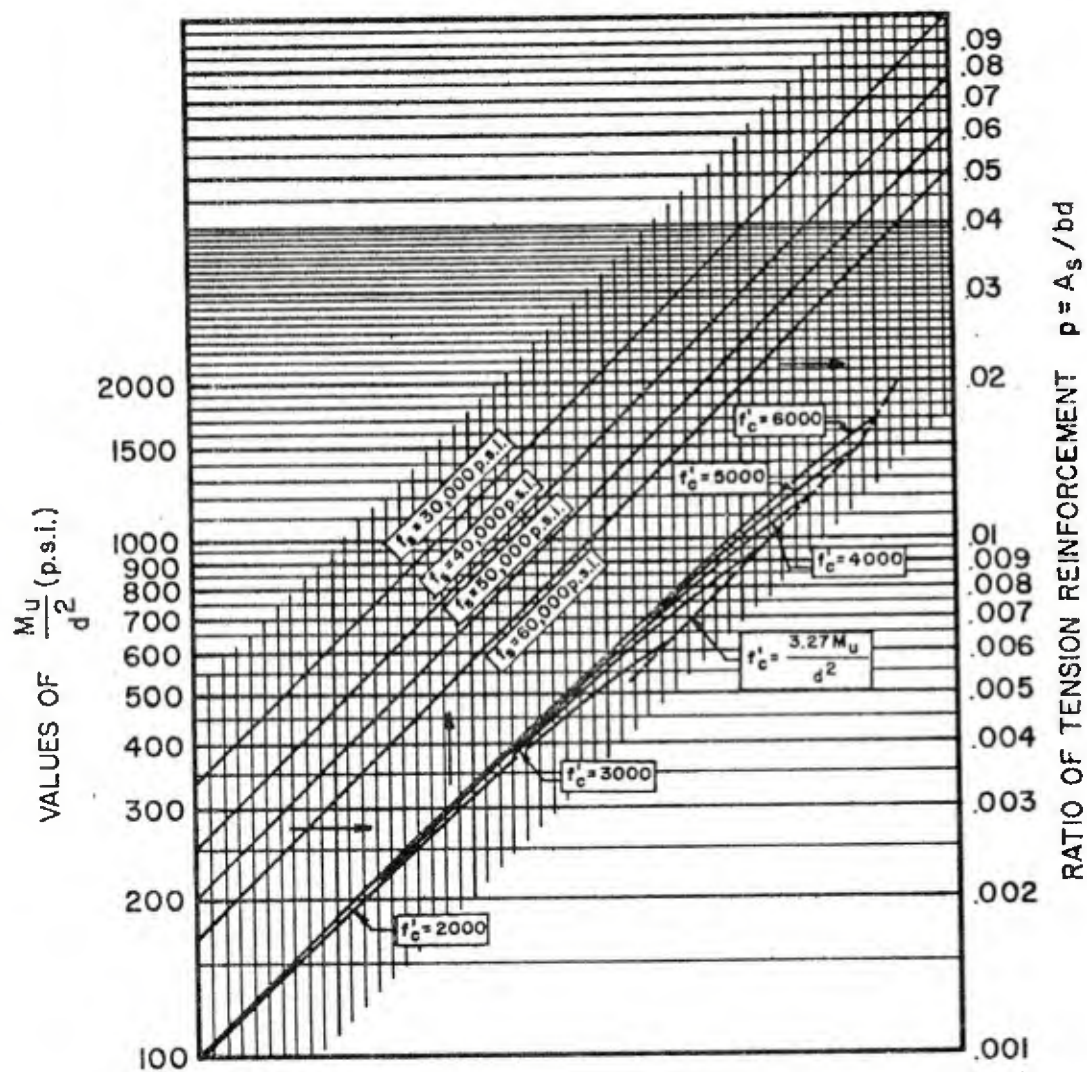


Figure 8. Moment capacity rectangular sections.

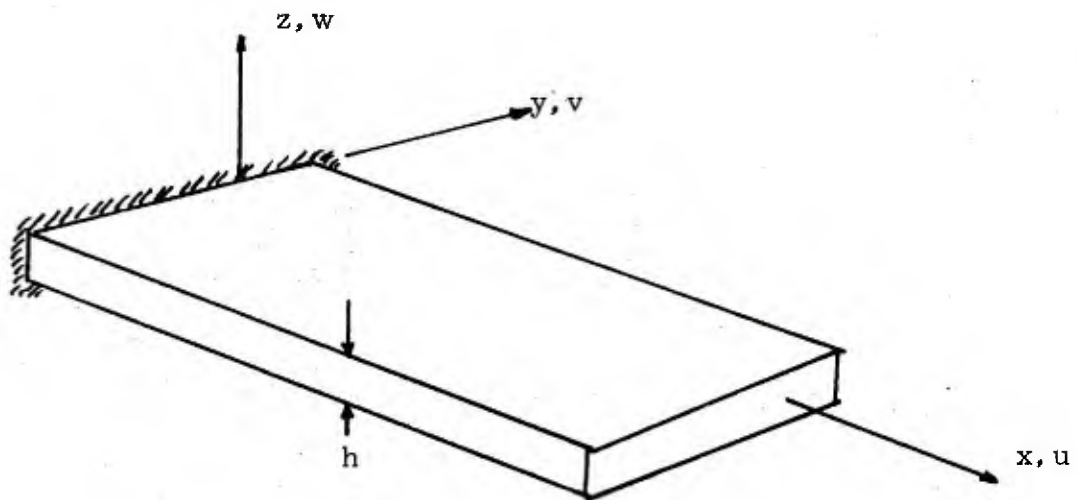


Figure 9 Reinforced concrete section

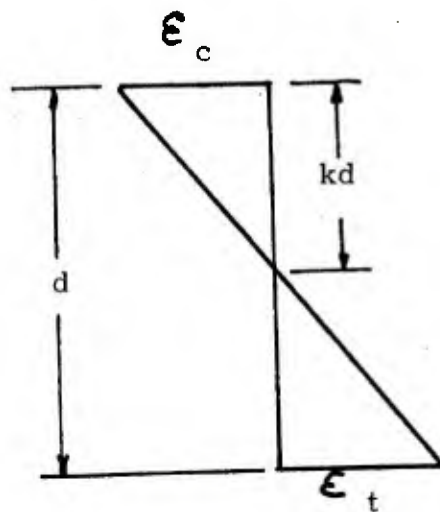


Figure 10. Strain distribution.

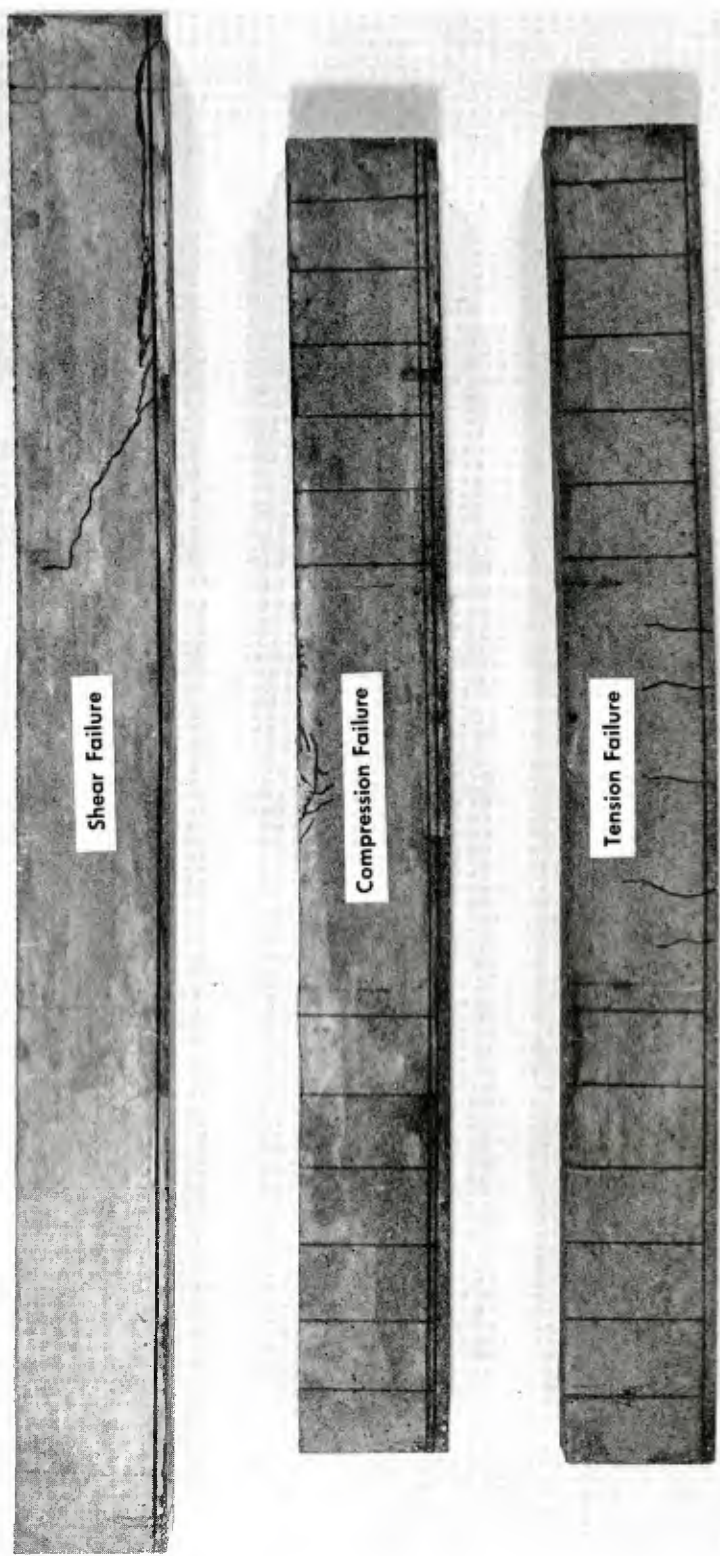
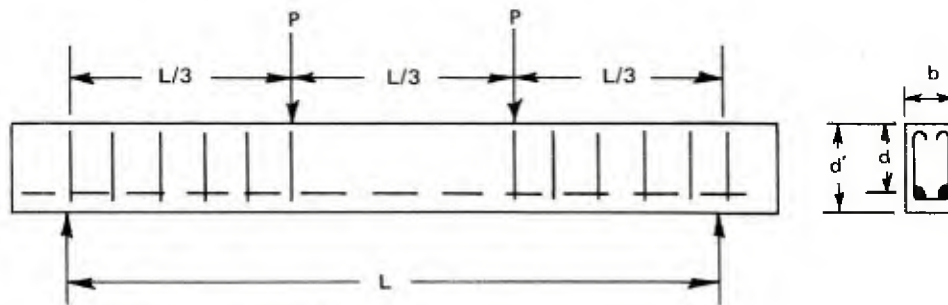


Figure 11 Model beams .



Length scale factor, $\alpha = 8$

Strength scale factor, $\beta = 3.7$

Type of failure—tension

Design Data

	Prototype	Model
L (in.)	135	16.87
b (in.)	8	1
d' (in.)	16	2
d (in.)	14.2	1.77
A_s (in. ²)	2 no. 7 1.20	2 12 gage 0.0187
f_y (psi)	85,000	23,000
f'_c (psi)	4,360	1,180
2 P (lb)	59,200	260

Test Results

Model	Material	Actual f'_c (psi)	Failure Load (lb)	Failure Mode	Deviation (%)
B-2-1	microconcrete	1,401	288	tension	+10
B-2-2	microconcrete	1,401	290	tension	+11
B-2-3	microconcrete	1,401	252	tension	-2
B-2-4	gypsum	1,156	270	tension	+4
B-2-5	gypsum	1,156	264	tension	+2

Figure 12. Design data and test results for beam 1.

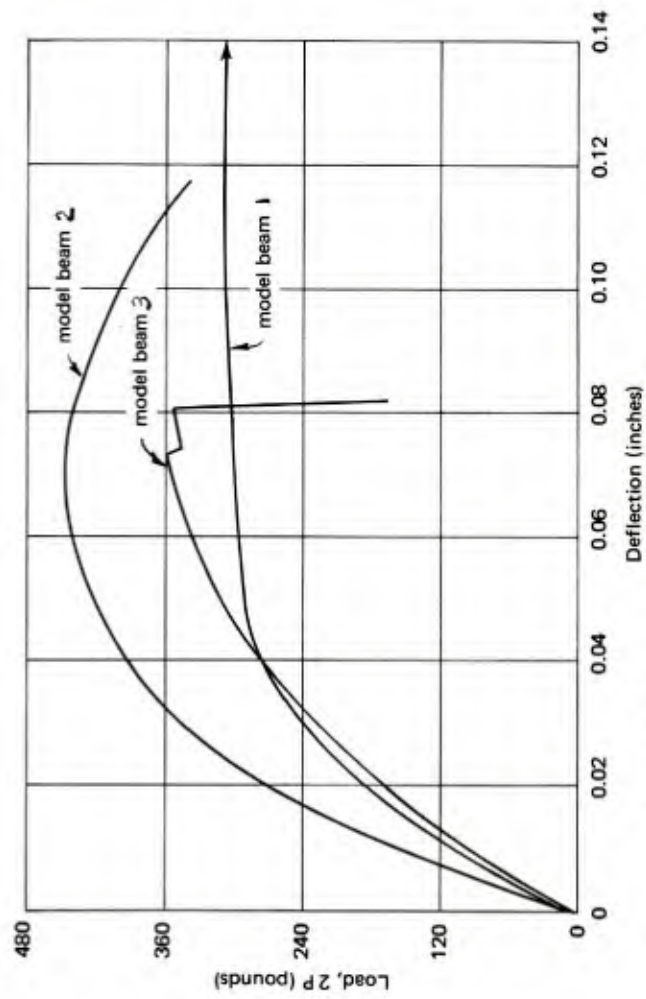
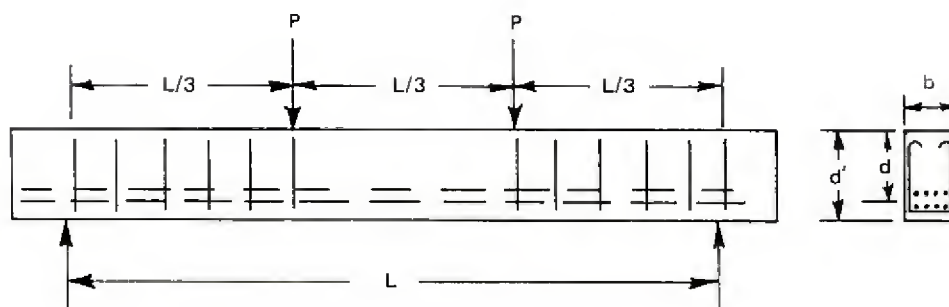


Figure 13. Load—deflection curves for various model beams.



Length scale factor, $\alpha = 8$

Strength scale factor, $\beta = 3.7$

Type of failure—compression

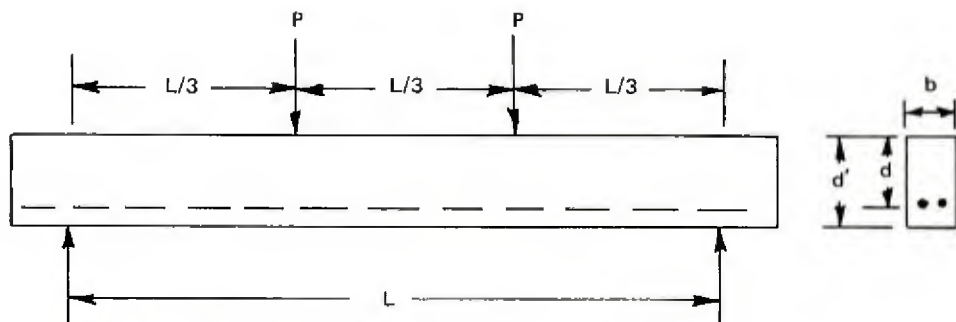
Design Data

	Prototype	Model
L (in.)	135	16.87
b (in.)	8	1
d' (in.)	16	2
d (in.)	13.4	1.67
A_s (in. ²)	8 no. 6 3.52	8 12 gage 0.055
f_y (psi)	86,400	23,000
f'_c (psi)	4,470	1,195
$2P$ (lb)	101,800	425

Test Results

Model	Material	Actual f'_c (psi)	Failure Load (lb)	Failure Mode	Deviation (%)
B-3-1	microconcrete	1,400	440	compression	+4
B-3-2	microconcrete	1,400	435	compression	+4
B-3-3	gypsum	1,165	506	compression	+10
B-3-4	gypsum	1,165	511	compression	+11
B-3-5	gypsum	1,165	538	compression	+17

Figure 14. Design data and test results beam 2.



Length scale factor, $\alpha = 6$

Strength scale factor, $\beta = 2$

Type of failure—shear

Design Data

	Prototype	Model
L (in.)	120	20
b (in.)	6	1
d' (in.)	12	2
d (in.)	10.75	1.62
A_s (in. ²)	2 no. 7 1.20	4 12 gage 0.0333
f_y (psi)	45 to 50,000	24,000
f'_c (psi)	5,970	1,490
$2P$ (lb)	24,000	333

Test Results

Model	Material	Actual f'_c (psi)	Failure Load (lb)	Failure Mode	Deviation (%)
B-4-1	microconcrete	1,489	342	shear	+3
B-4-2	microconcrete	1,489	364	shear	+9
B-4-3	microconcrete	1,489	370	shear	+11
B-4-4	gypsum	1,428	349	shear	+5
B-4-5	gypsum	1,428	360	shear	+8
B-4-6	gypsum	1,428	360	shear	+8

Figure 15. Design data and test results for beam 3.

a Point at which equilibrium chek stopped solution

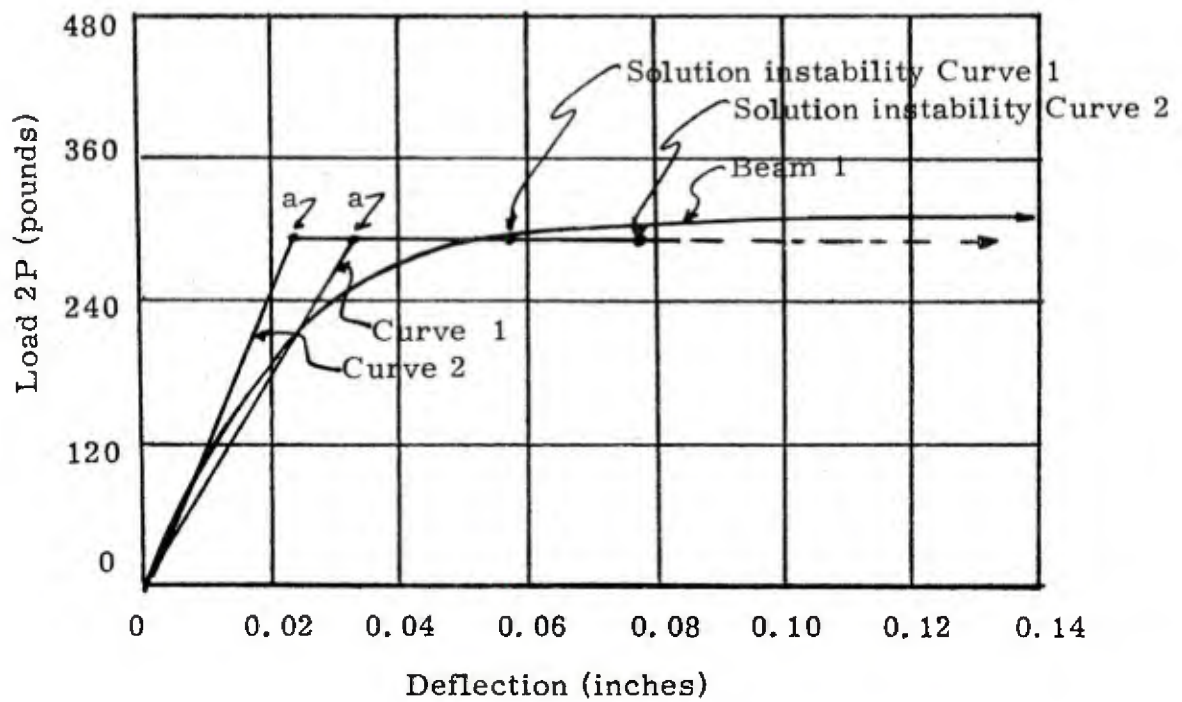


Figure 16 Load- Deflection curve for Tension failure

a Stiffness not positive definite(no equilibrium check)

b Solution terminated iteration will not converge

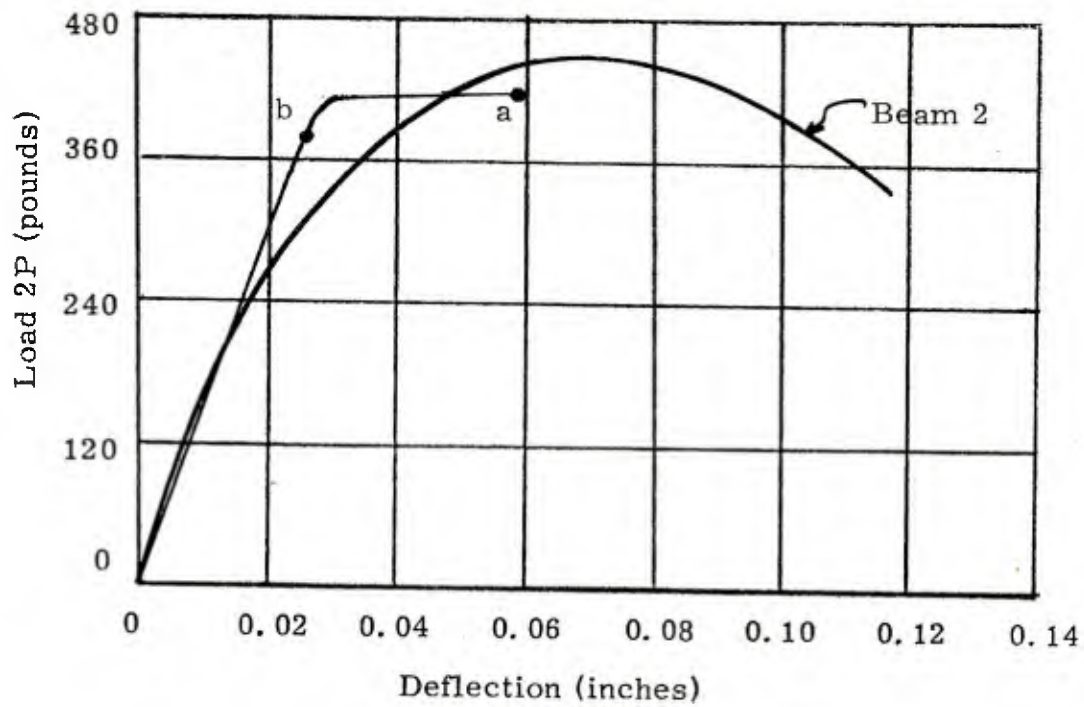


Figure 17 Load - deflection curves for compression failure.

A) Solution by applied force

B) Solution by applied displacement

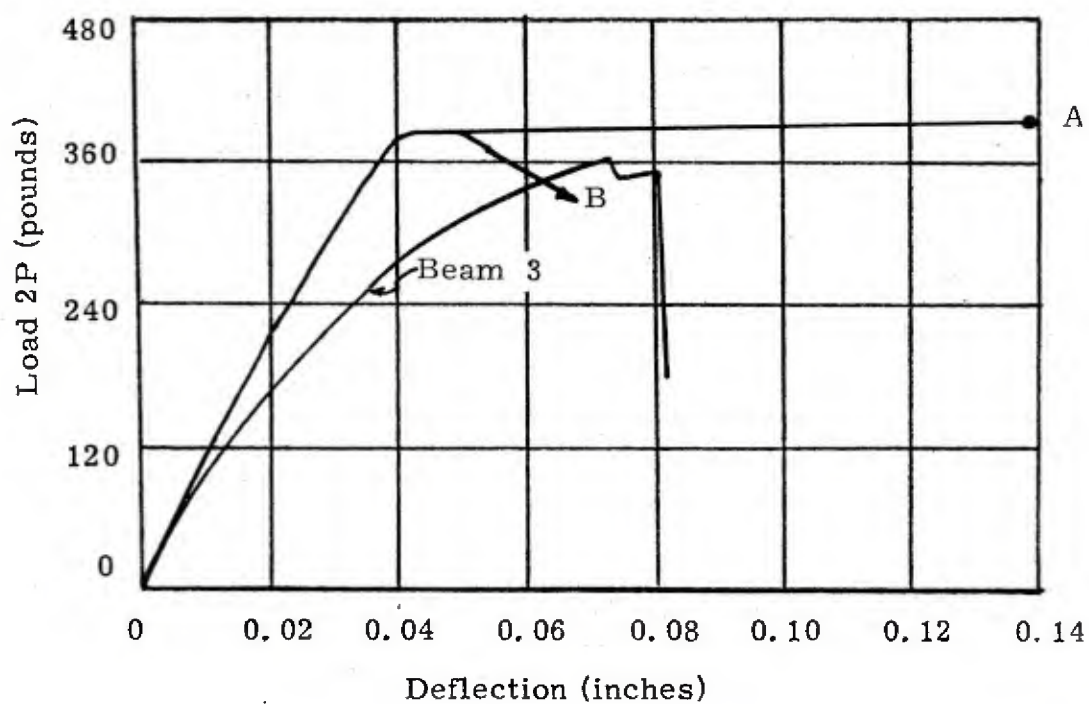


Figure 18 Load - deflection curves for shear failure.

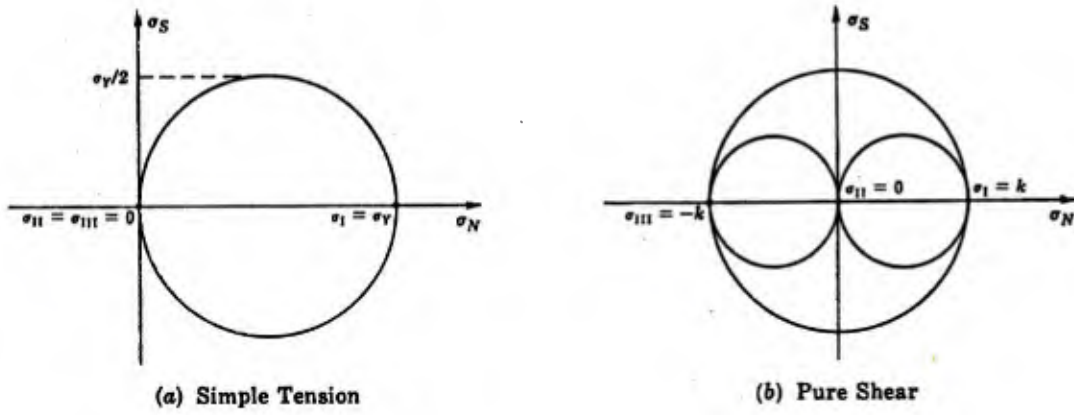


Figure 19. Tresca yield condition.

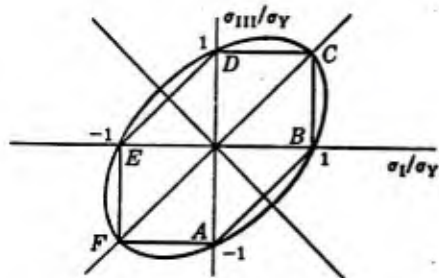


Figure 20. Comparison of Tresca and Von Mises yield condition.

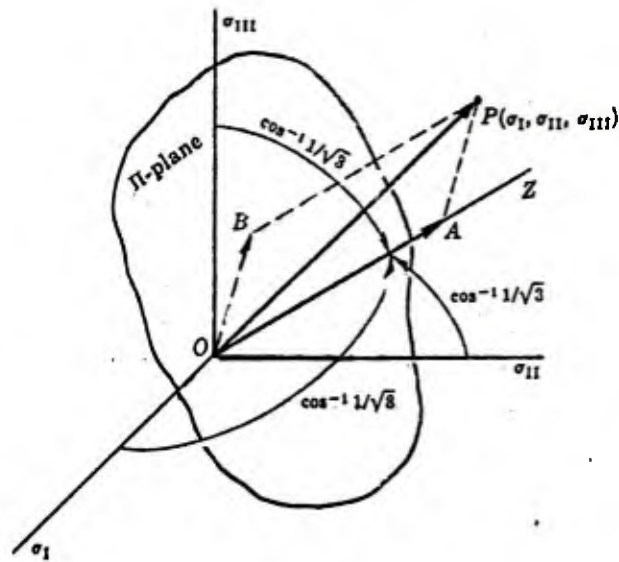


Figure 21 Pi Plane.

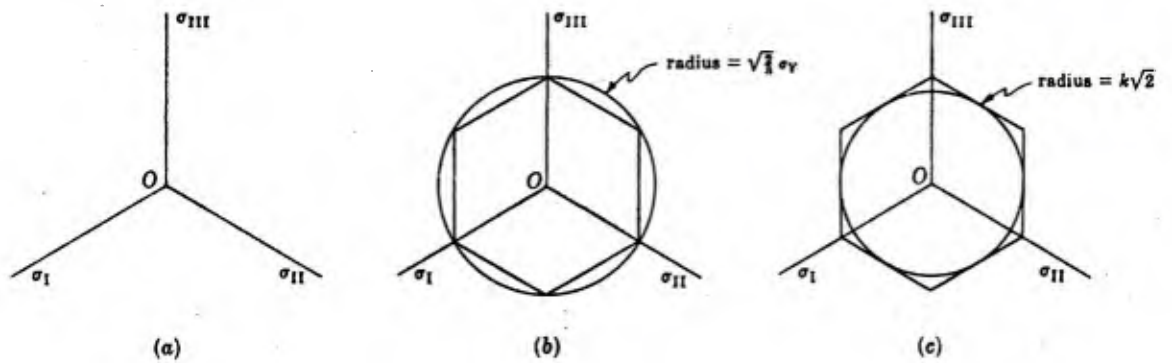


Figure 22. Yield surface.

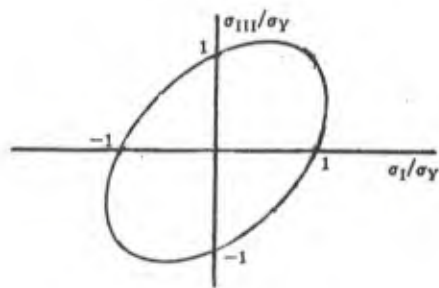


Figure 23 Drucker - Prager yield condition.

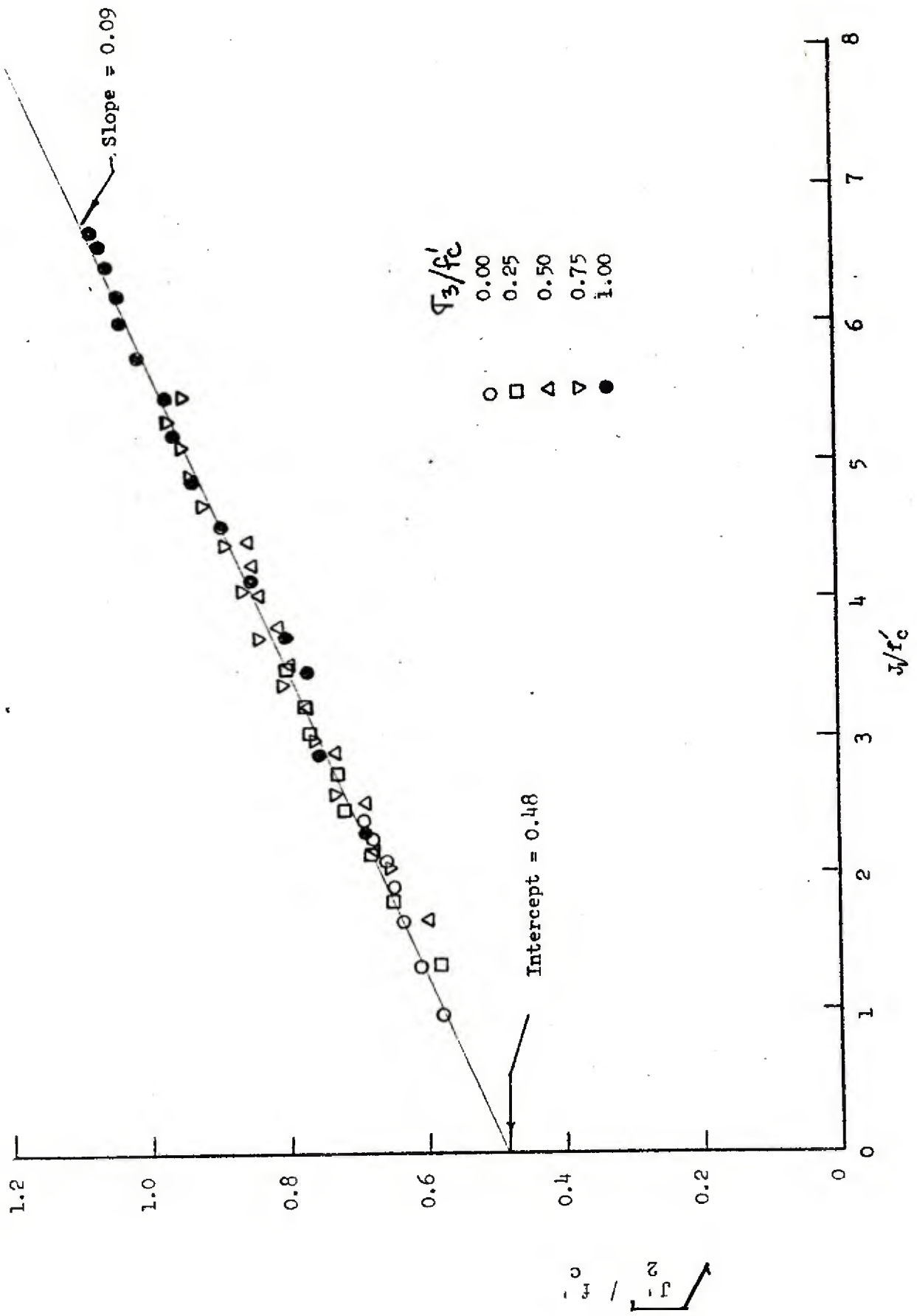


Figure 24 Drucker - Prager failure envelope.

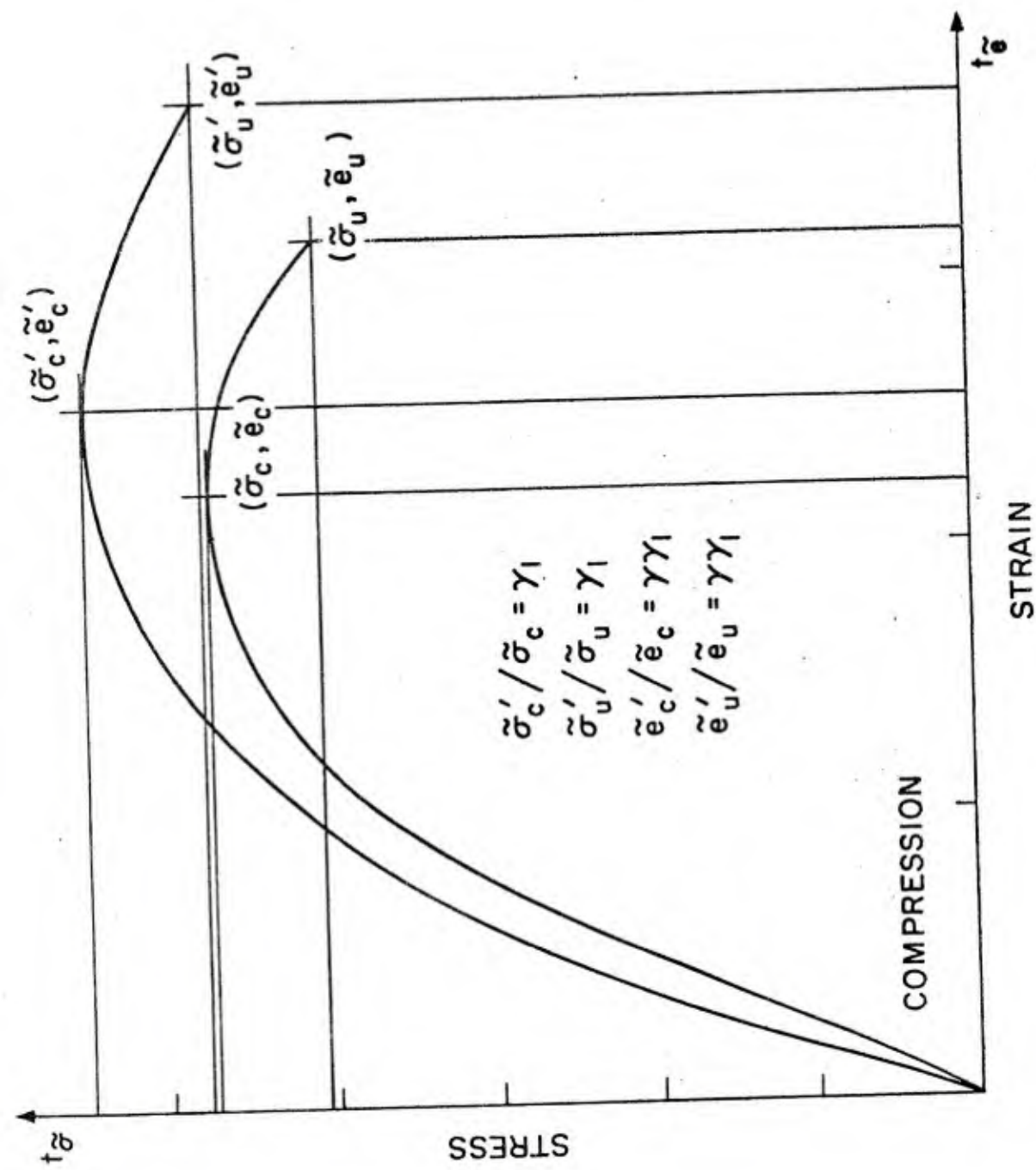


Figure 25a. Increase of strength parameters under multiaxial conditions.

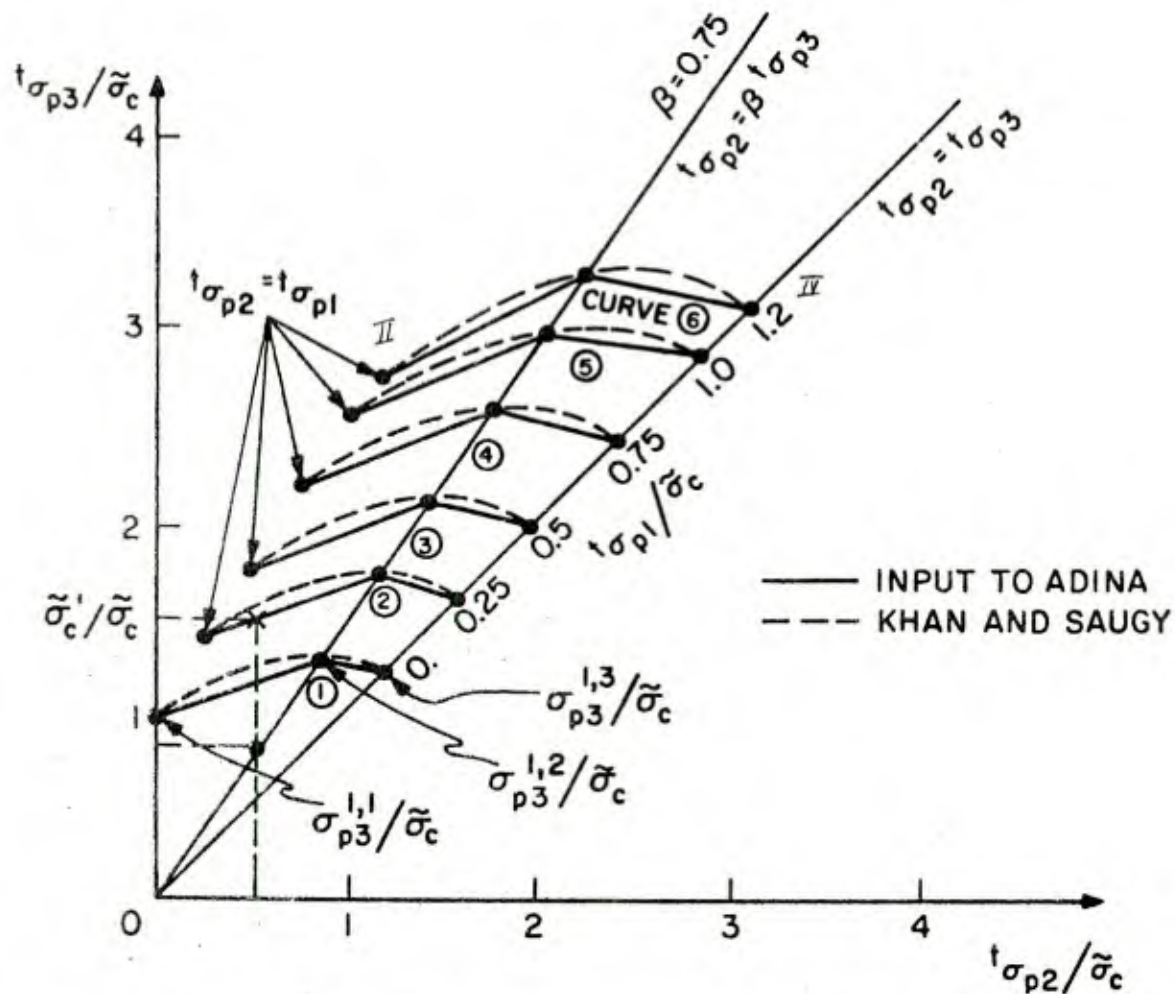


Figure 25b. Triaxial concrete compressive failure envelope.

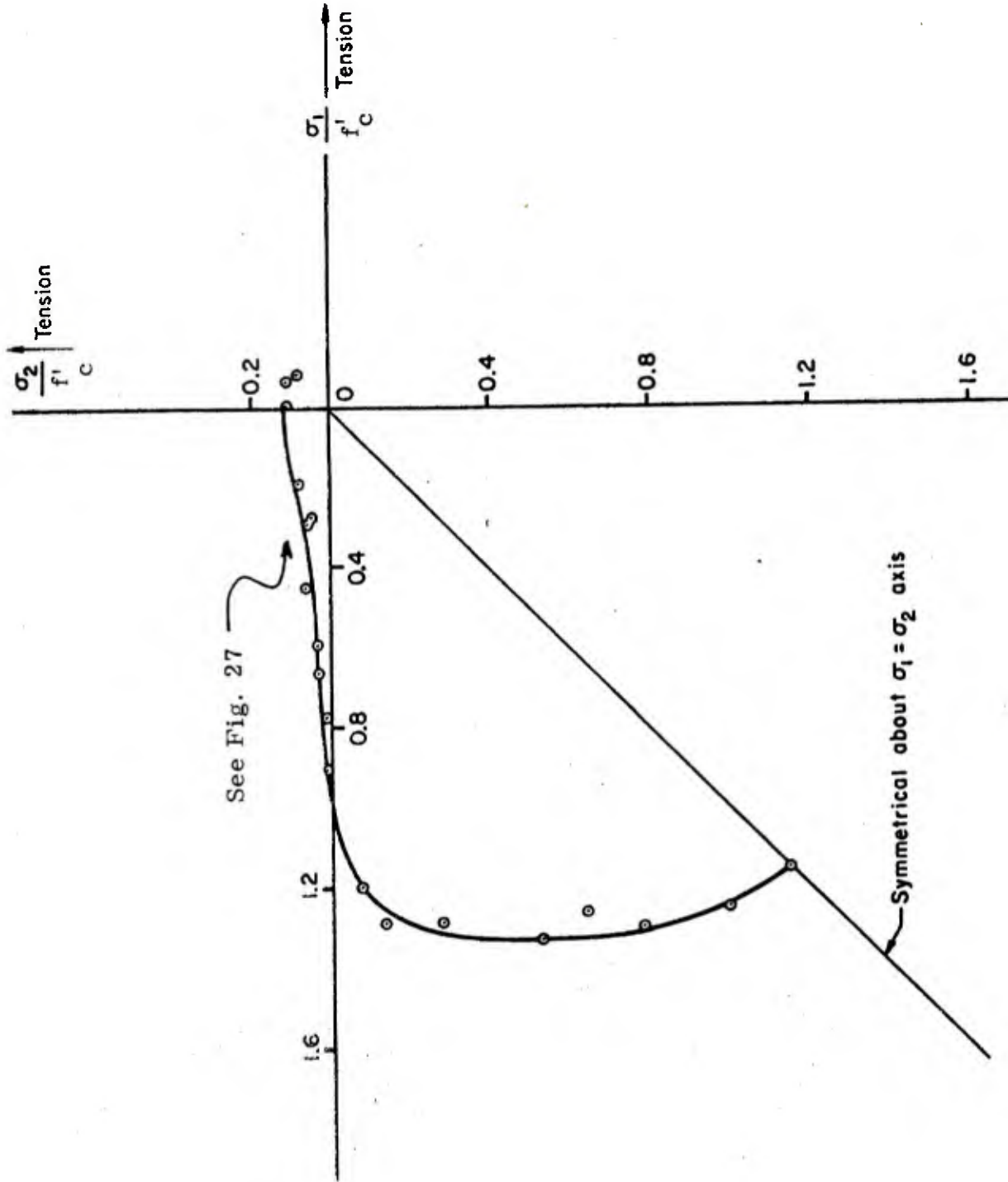


Figure 26. Biaxial strength of concrete.

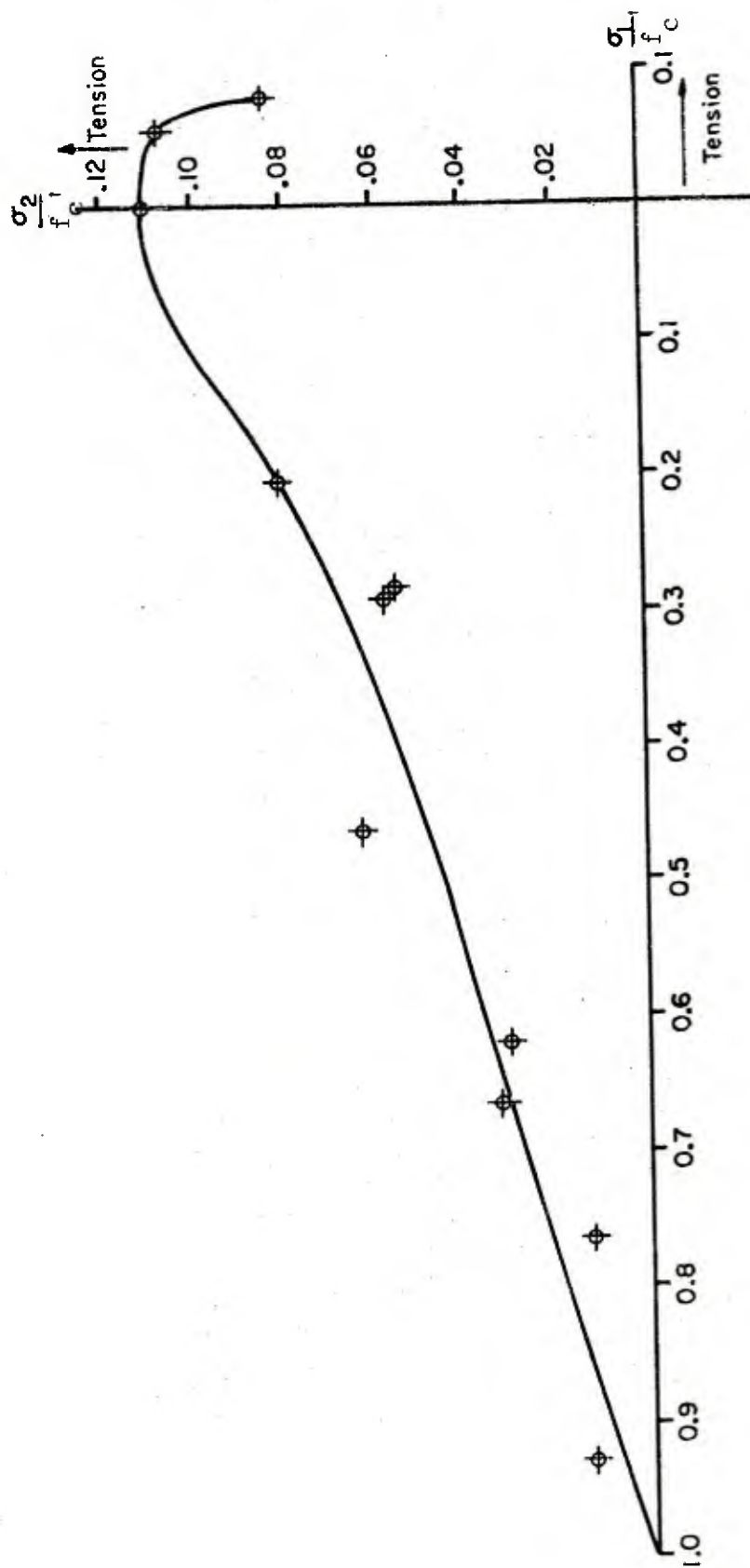


Figure 27. Biaxial tension and tension-compression strength data.

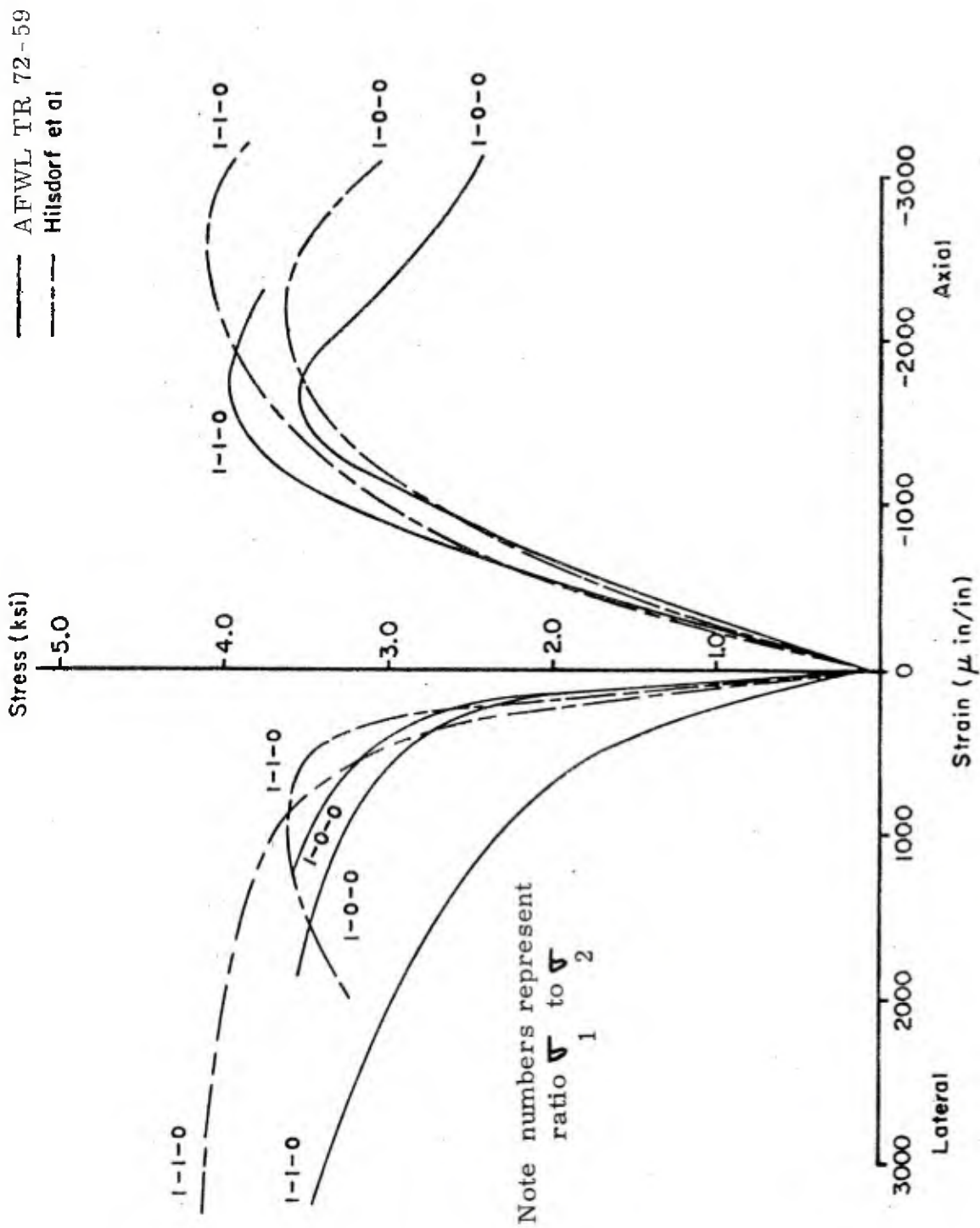


Figure 28. Uniaxial and biaxial compression stress-strain curves.



Figure 29. Normalized triaxial compression data.

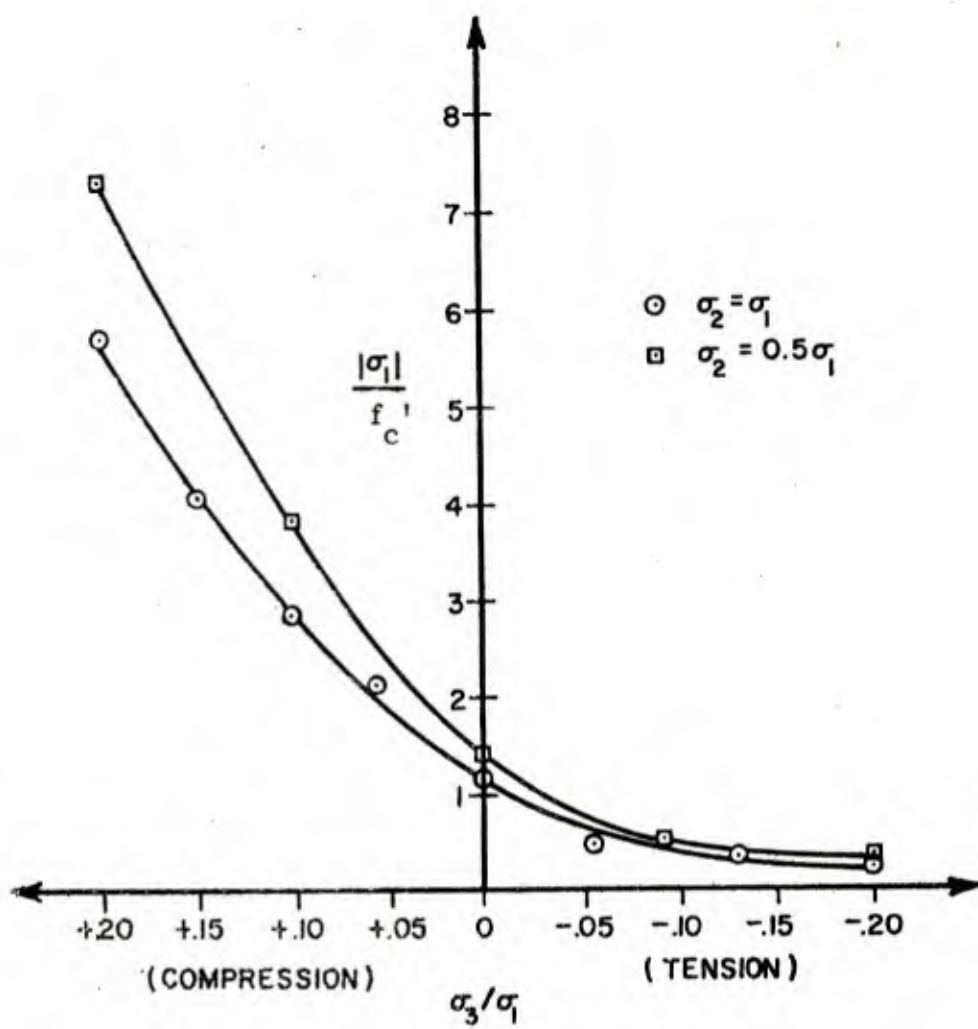
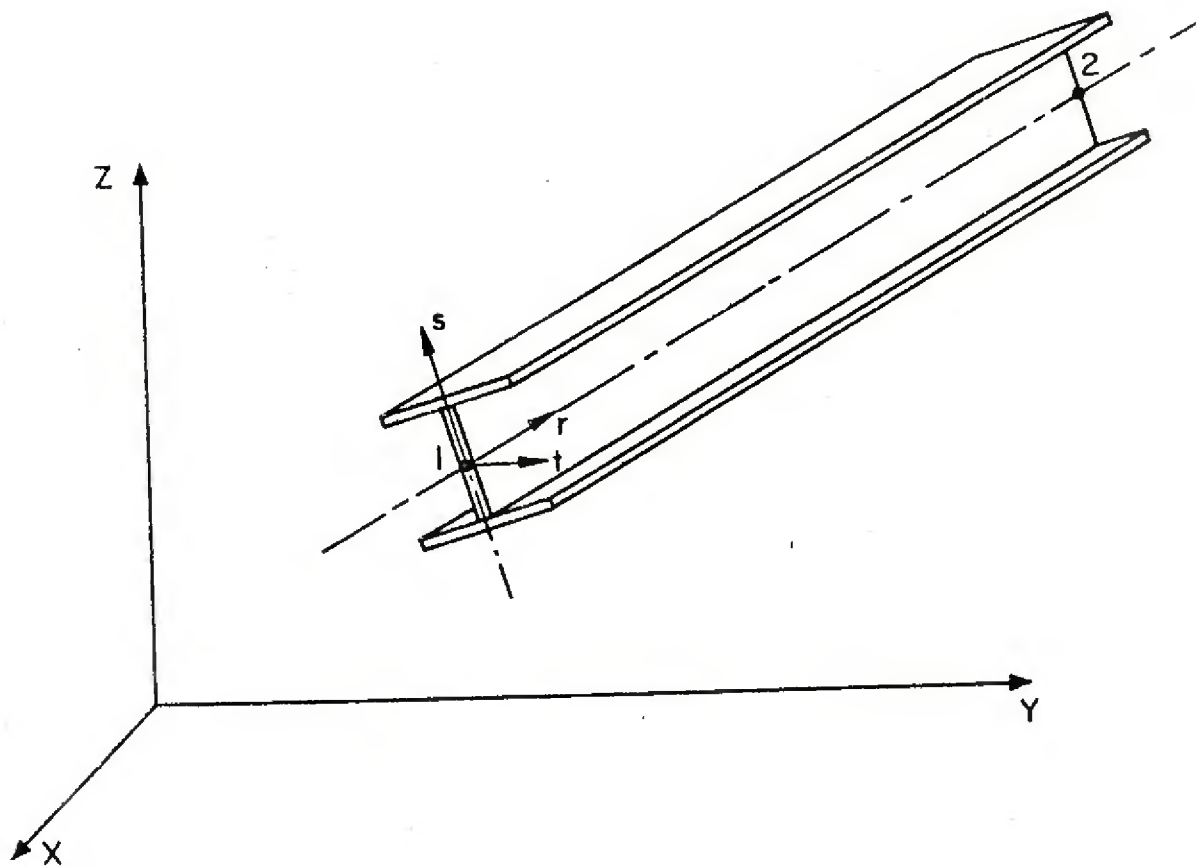


Figure 30. Triaxial concrete strength for ratios of $\frac{\sigma_3}{\sigma_1}$.



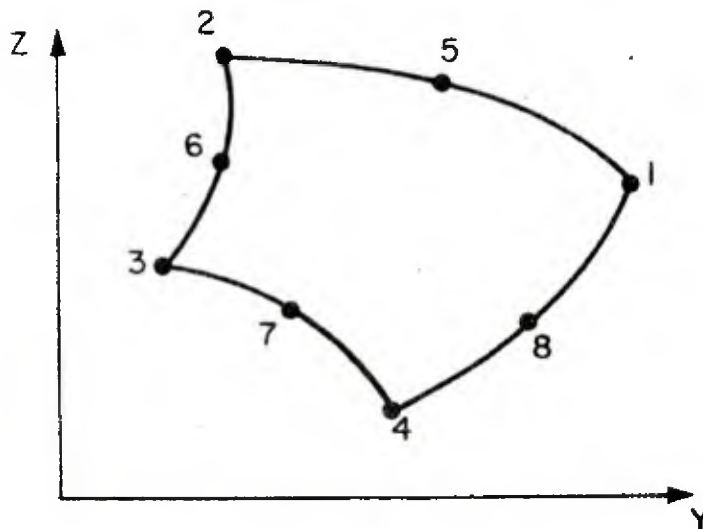
AVAILABLE NONLINEAR FORMULATIONS

- a. LINEAR ANALYSIS
- b. MATERIALLY NONLINEAR ONLY
- c. UPDATED LAGRANGIAN WITH LARGE DISPLACEMENTS BUT SMALL STRAINS

AVAILABLE MATERIAL MODELS

- a. ISOTROPIC LINEAR ELASTIC
- b. ELASTIC-PLASTIC (PERFECTLY-PLASTIC OR ISOTROPIC STRAIN HARDENING, RECTANGULAR AND PIPE SECTION)

Figure 31. Beam elements.



AVAILABLE NONLINEAR FORMULATIONS

- a. LINEAR ANALYSIS
- b. MATERIALLY NONLINEAR ONLY
- c. UPDATED LAGRANGIAN
- d. TOTAL LAGRANGIAN

AVAILABLE MATERIAL MODELS

- a. ISOTROPIC LINEAR ELASTIC
- b. ORTHOTROPIC LINEAR ELASTIC
- c. ISOTROPIC THERMO-ELASTIC
- d. CURVE DESCRIPTION NONLINEAR MODEL FOR ANALYSIS OF GEOLOGICAL MATERIALS (INCLUDING TENSION CUT-OFF AND TENSION RELEASE)(plane strain and axisymmetric only)
- e. CONCRETE MODEL (INCLUDING CRACKING AND CRUSHING)
- f. ISOTHERMAL PLASTICITY MODELS; VON MISES YIELD CONDITION (ISOTROPIC OR KINEMATIC HARDENING) OR DRUCKER-PRAGER YIELD CONDITION
- g. THERMO-ELASTIC-PLASTIC and CREEP MODELS VON MISES YIELD CONDITION (ISOTROPIC OR KINEMATIC HARDENING)
- h. ISOTROPIC NONLINEAR ELASTIC, INCOMPRESSIBLE (MOONEY-RIVLIN MATERIAL) (plane stress only)

Figure 32. Two-dimensional plane elements.

a Concrete model

b Variable modulus model

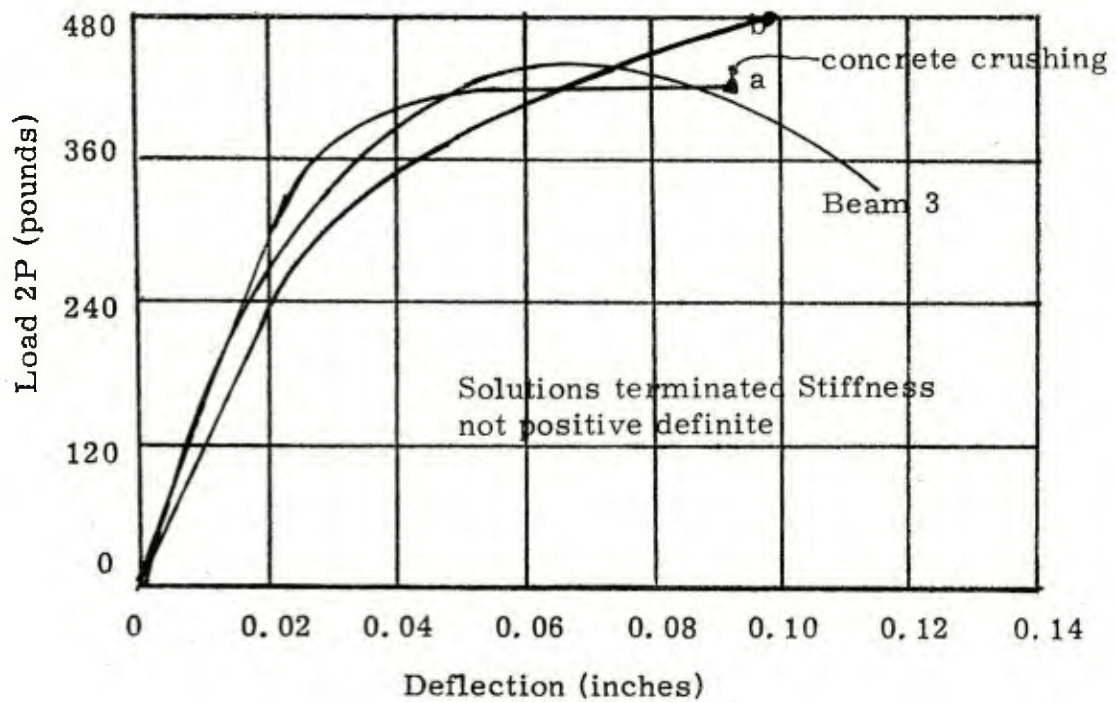


Figure 33 Load - deflection for compression failure beam

a Solution terminated stiffness not positive definite

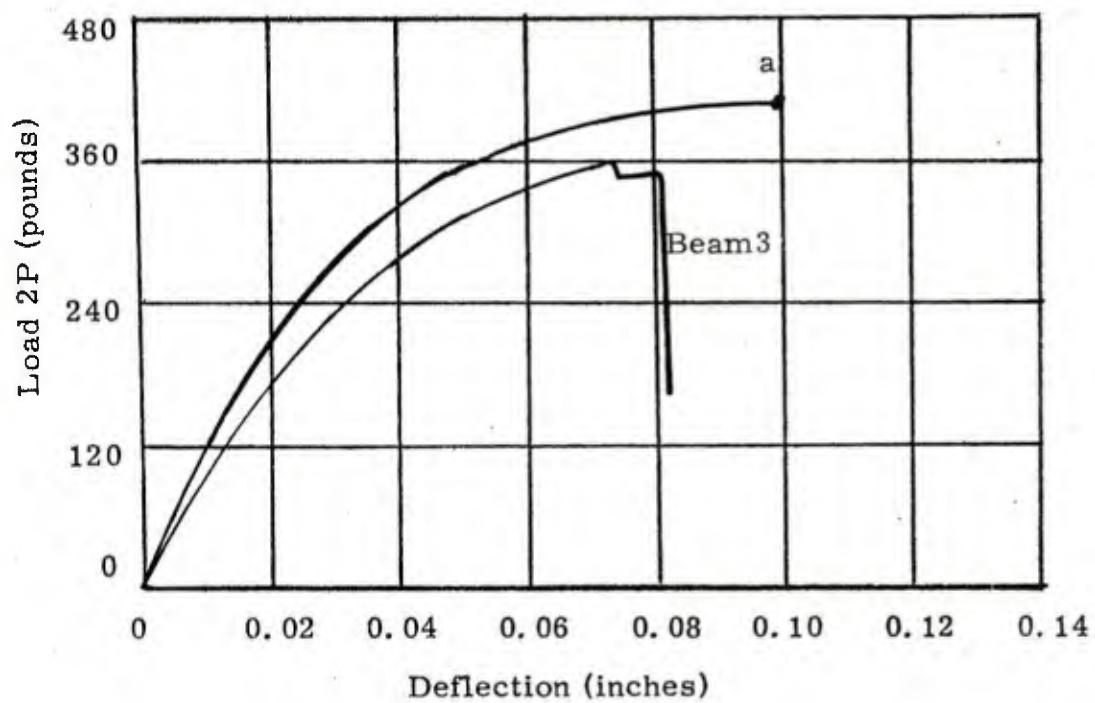


Figure 34. Load-deflection curves for shear failure.

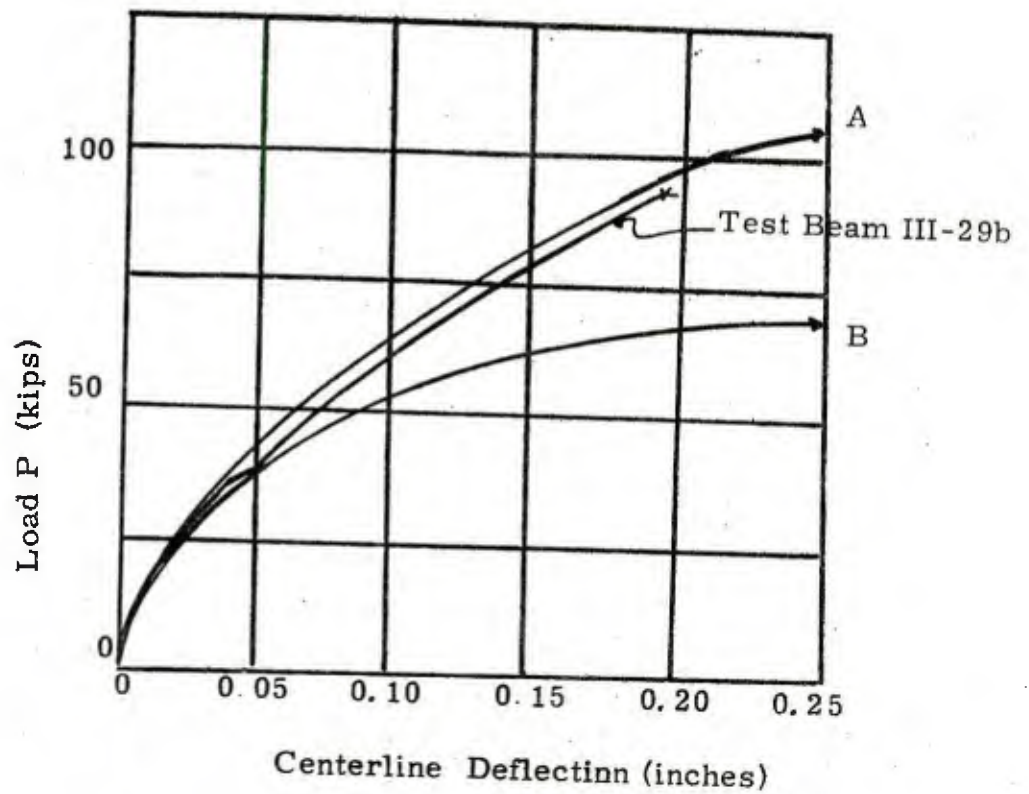
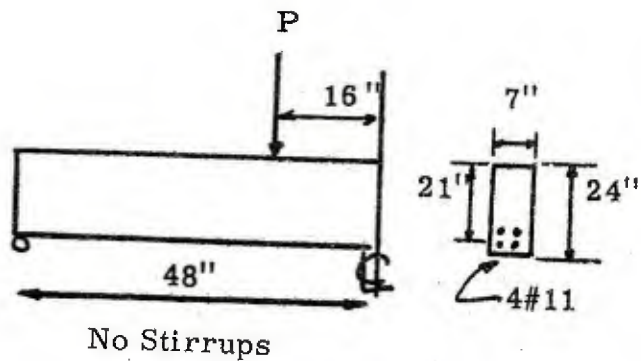
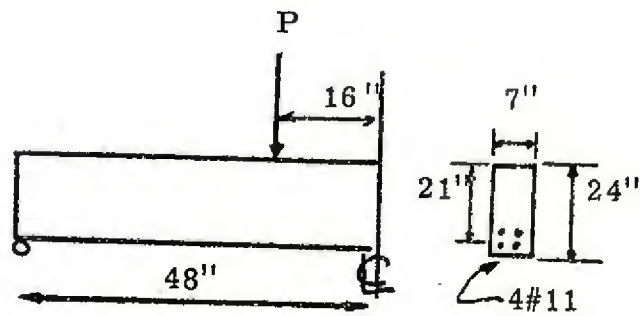


Figure 35 Results for beam without stirrups.



Stirrups #3 @ 6"

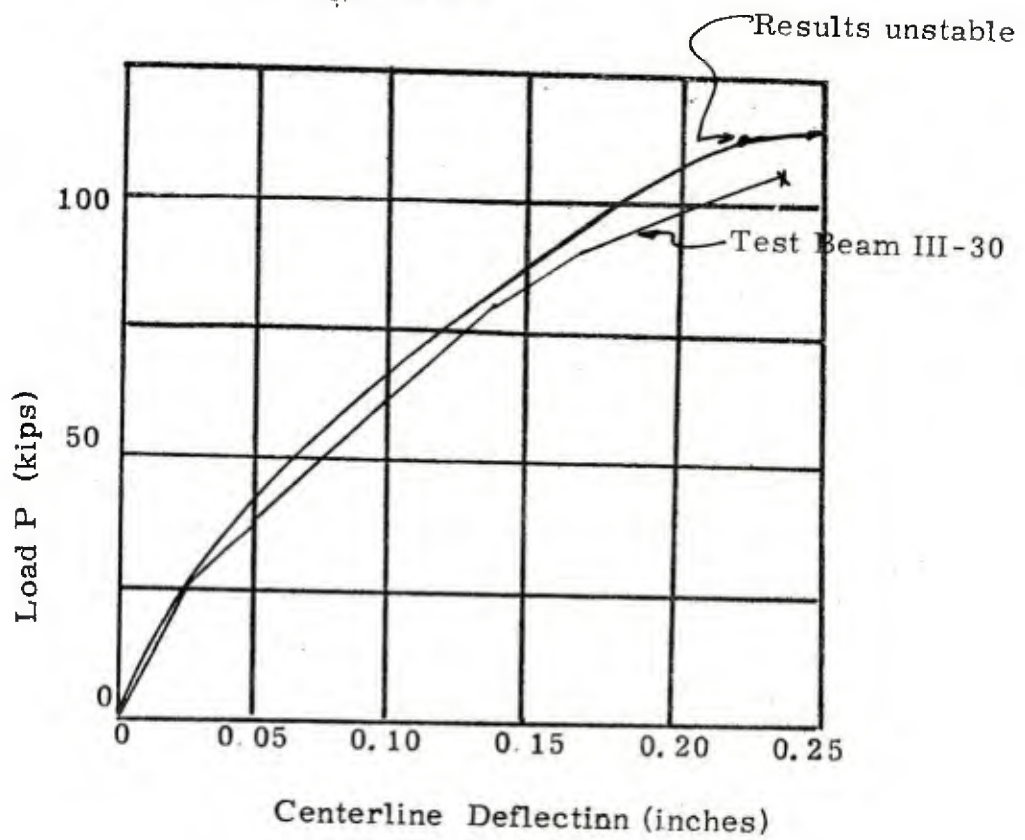
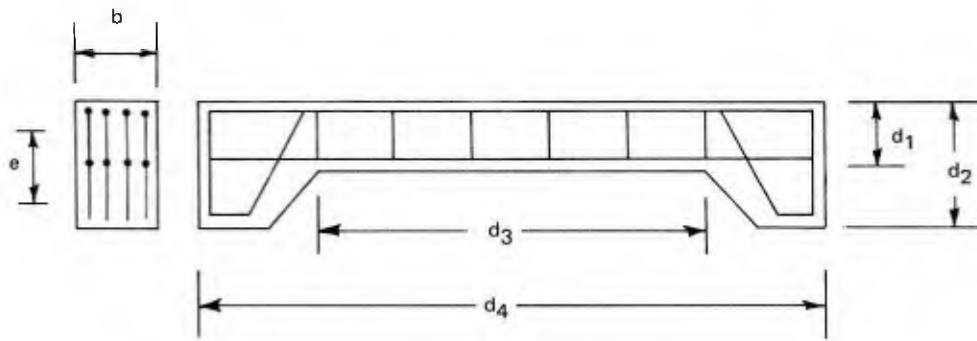


Figure 36 Results for beam with stirrups.



Length scale factor, $\alpha = 10$

Strength scale factor, $\beta = 1/1.45$

Design Data

	Prototype	Model
d_1 (in.)	10	1
d_2 (in.)	21.5	2.15
d_3 (in.)	50	5
d_4 (in.)	75	7.5
b (in.)	10	1
f_y (psi)	46,000	46,000/30,000
f'_c (psi)	varies	varies
D_s	5/8 in.	16 gage

Test Results

Model	Type	f_c (psi)	Eccentricity, e (in.)	Load (lb)	Failure Mode	Deviation From Scaled Prototype Value (%)	Prototype Number
C-1	direct	5,380	0	3,075	bearing	-24	A-6-a
C-2	direct	5,380	0.25	2,665	compression	-3	A-7-a
C-3	direct	5,380	0.25	2,740	compression	0	A-7-a
C-4	direct	5,380	0.75	830	tension	-8	A-9-a
C-5	direct	5,380	1.25	425	tension	-1	A-10-b
C-6	strength reduction	2,450	0	2,400	bearing	-17	B-6-b
C-7	strength reduction	2,450	0.25	2,125	compression	+20	B-7-b
C-8	strength reduction	2,450	1.25	350	tension	+10	B-10-b

Figure 37. Design data and test results for beam-columns.

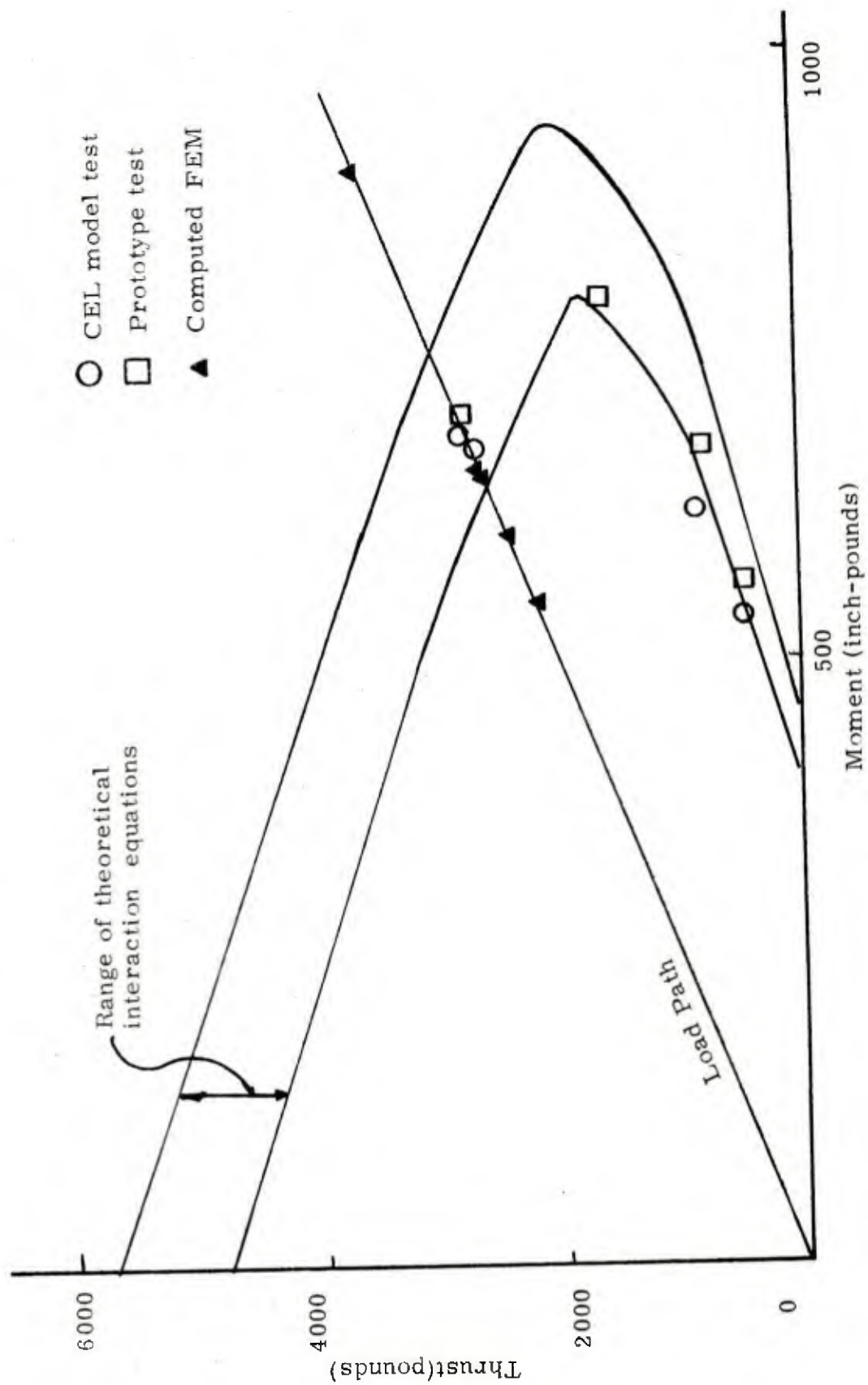


Figure 38. Experimental and computed thrust-moment data points.

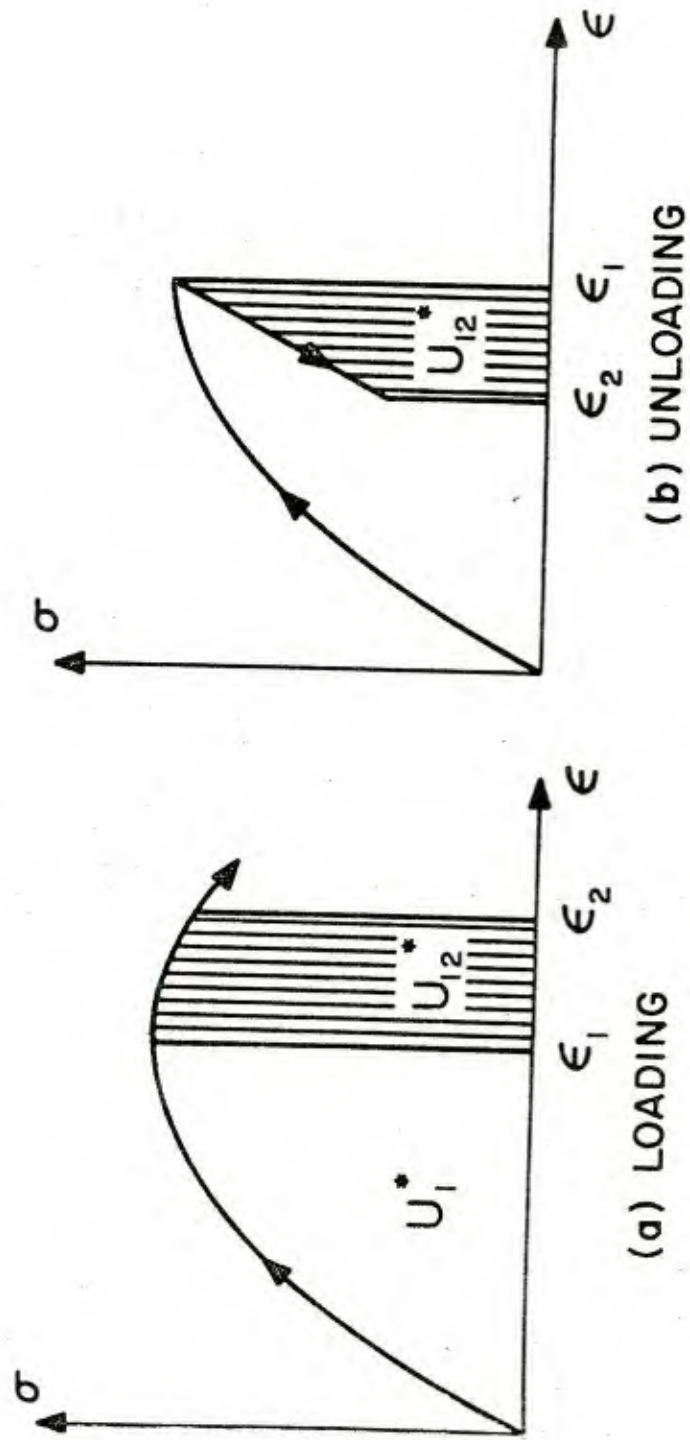


Figure 39. Internal energy density relation SINGER.

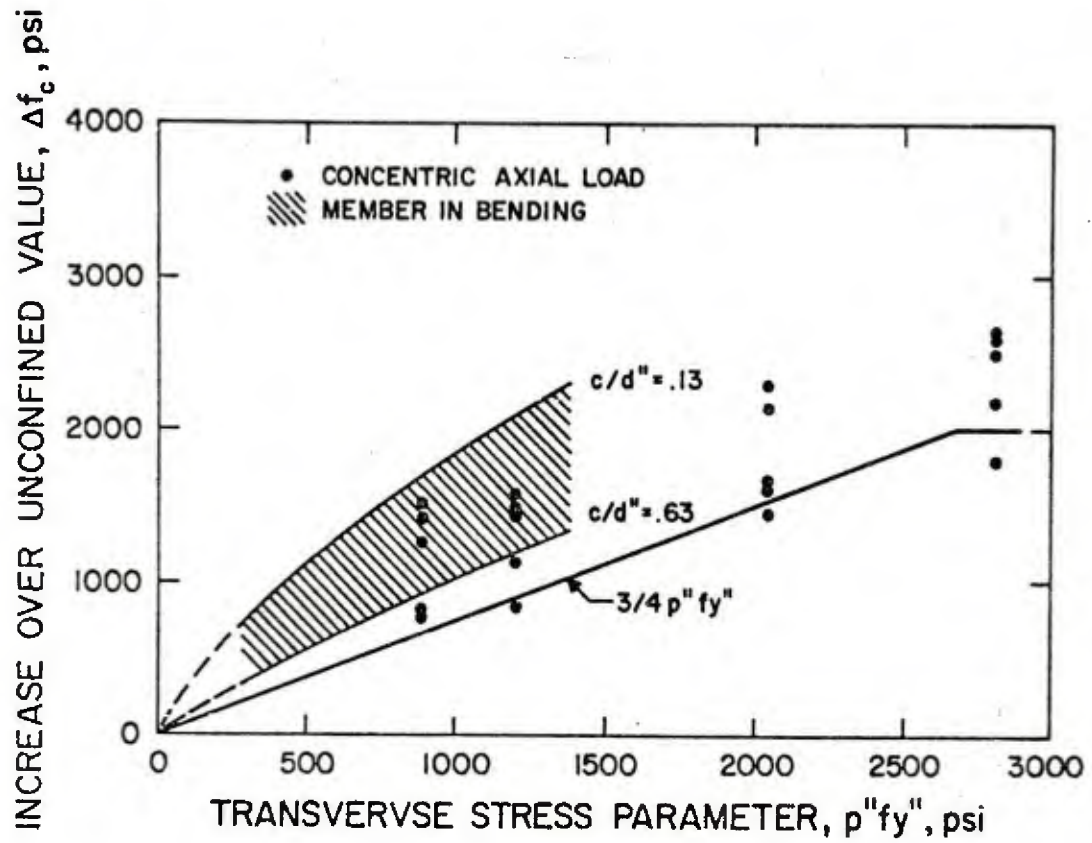


Figure 41. Ultimate strength for confined concrete.

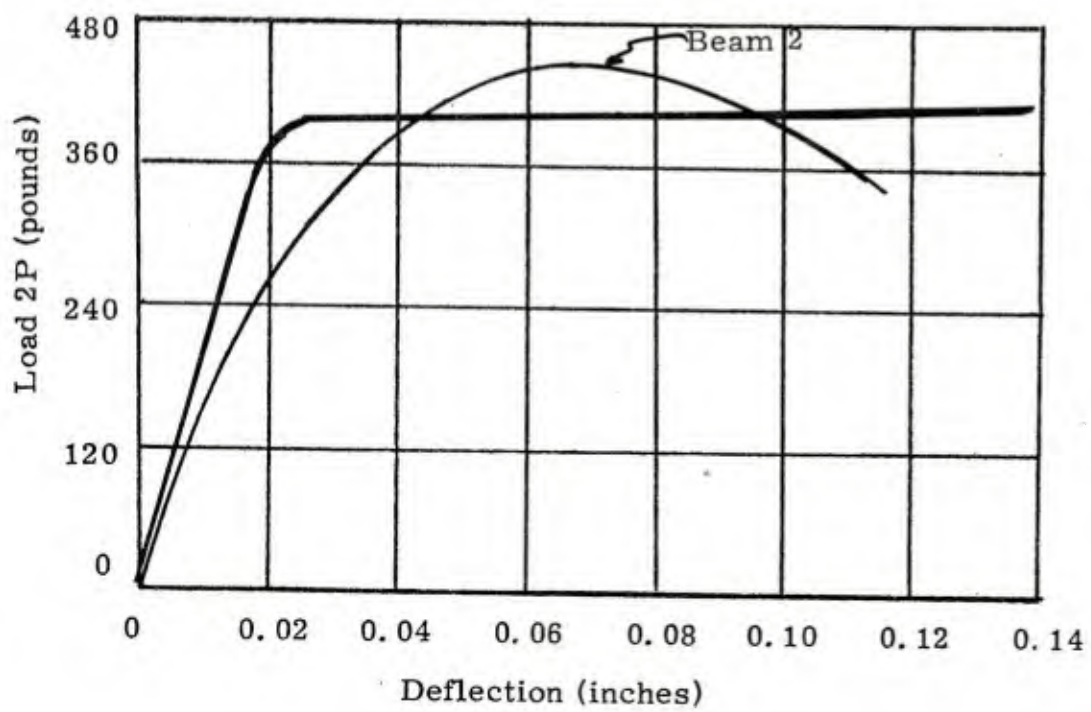


Figure 42 Load - deflection curves compression failure(SINGER).

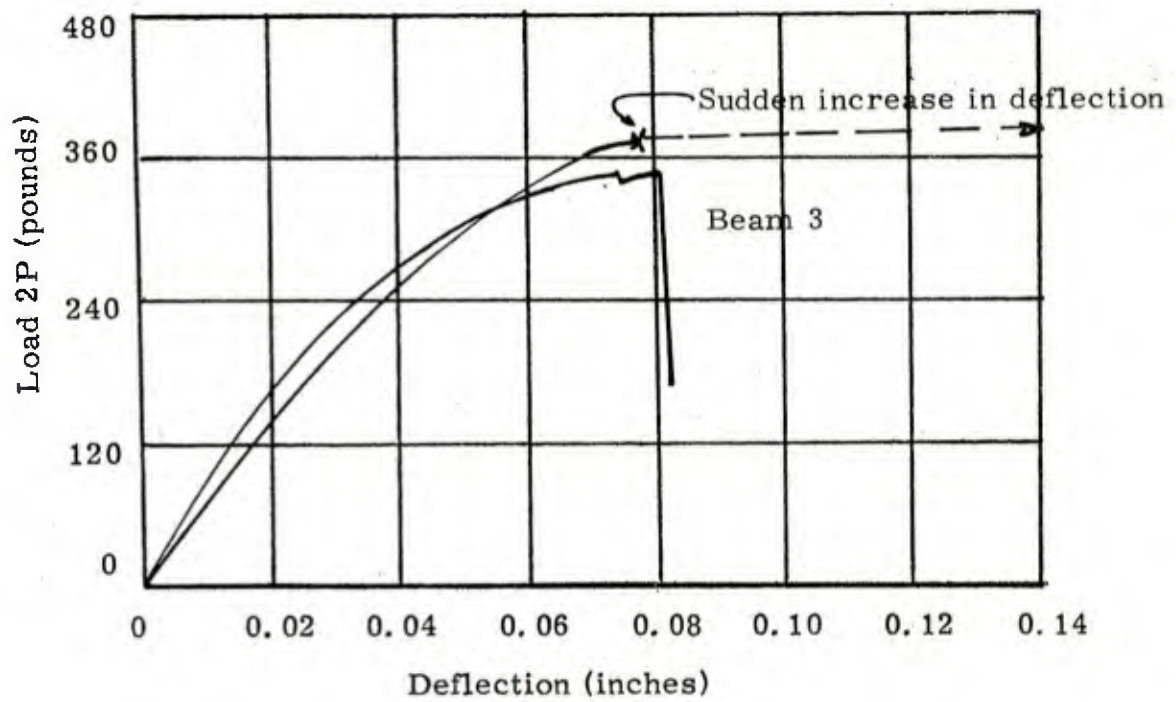


Figure 43 Load - deflection curves shear failure(SINGER)

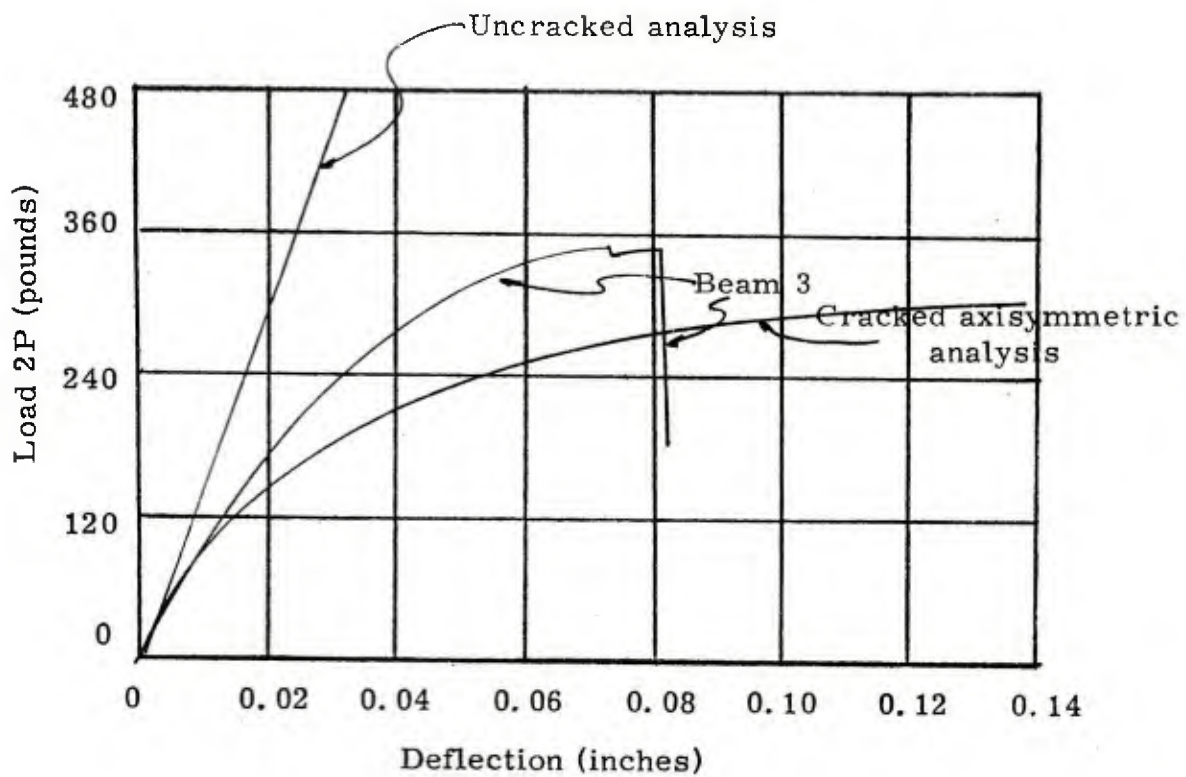


Figure 44. Results of MARC analysis.

NCEL
TM-
51-78-18

c,2

LIBRARY
NAVAL CIVIL ENGINEERING LABORATORY
PORT HUENEME, CA 93043